Energy, Mines and Resources Canada
Énergie, Mines et Ressources Canada

CANMET

Canada Centre for Mineral and Energy Technology
Centre canadien de la technologie des minéraux et de l'énergie

Mining Research Laboratories
Laboratoires de recherche minière

THE POST-FAILURE BEHAVIOUR OF THE LAC DU BONNET GRANODIORITE

J.S.O. Lau and B. Gorski

September 1991

Mining Research Laboratories
Divisional Report MRL 91-098(TR)

Canada

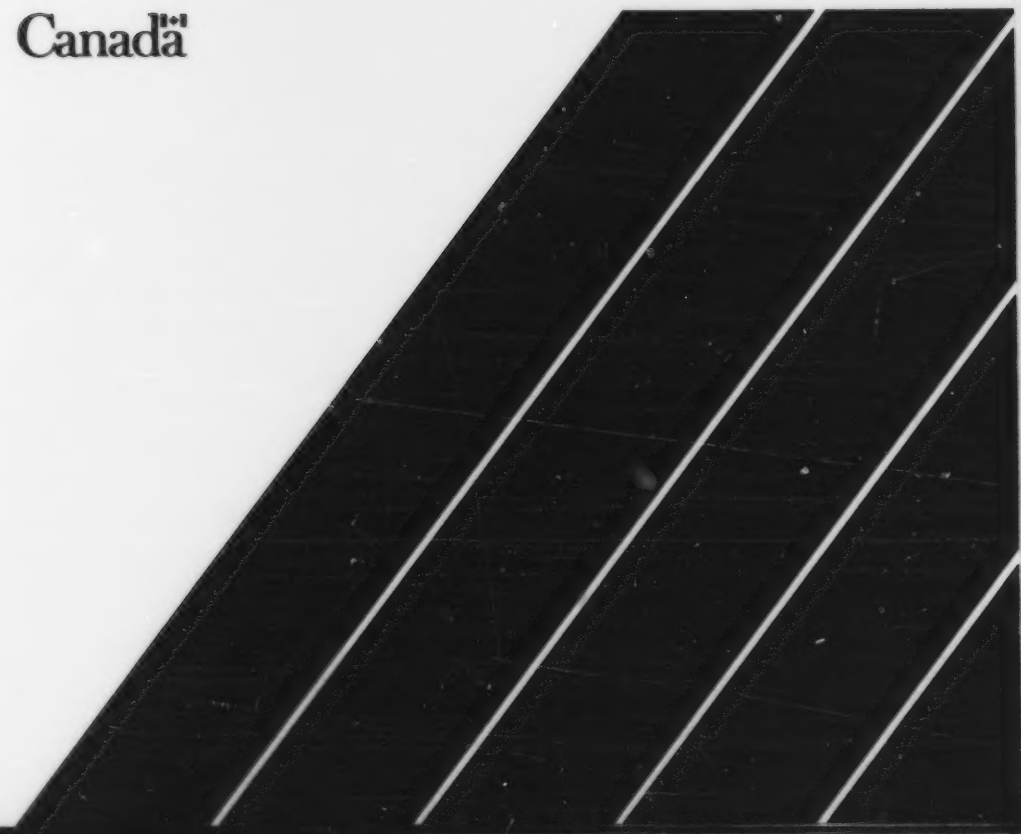

92-01198/

THE POST-FAILURE BEHAVIOUR OF THE LAC DU BONNET GRANODIORITE

J.S.O. Lau and B. Gorski September 1991

Mining Research Laboratories
Divisional Report MRL 91-098(TR)

This document is an unedited interim report prepared primarily for its sponsor and intended for restricted release. It does not represent a final expression of the opinion of the Canada Centre for Mineral and Energy Technology (CANMET)

Ce document est un rapport provisoire non-révisé et rédigé principalement pour la diffusion restreinte à son commanditaire. Il ne représente nullement l'expression définitive de l'opinion du Centre canadien de la technologie des minéraux et de l'énergie (CANMET)

59 pp

MICROMEDIA

THE POST-FAILURE BEHAVIOUR OF THE LAC DU BONNET GRANODIORITE

by

J.S.O. Lau[1] and B. Gorski[2]

ABSTRACT

A laboratory testing program was carried out to study the post-failure behaviour of the Lac du Bonnet granodiorite obtained from the 420 Level of the URL. The rock was found to exhibit class II behaviour. The development of cracks in the specimens appeared to start at a stress level in the range of 35 - 45% of the peak strength. The onset of dilation appeared to occur at a stress level equivalent to approximately 65 - 75% of the peak strength.

The peak strength increased with confining pressure. The predicted uniaxial compressive strength, σ_c, and the material constant, m, in the Hoek and Brown failure criterion for the granodiorite were found to be 224 MPa and 26.27 respectively.

As the confining pressure increased, the failure mode changed from cracks and conjugate fractures to a single open shear fracture. The inclination angle, β, of the fracture plane with the specimen axis increased slightly with increasing confining pressure as predicted.

Crack closure caused the tangent Young's modulus and Poisson's ratio to increase as the confining pressure was raised from 0 to 10 MPa. However, development and growth of cracks caused the modulus to decrease and the Poisson's ratio to increase at peak strength.

Keywords: post-failure, uniaxial, triaxial, stress-strain, peak strength, failure criterion, angle β, tangent Young's modulus, Poisson's ratio

---

[1]Geotechnical Engineer, AECL Research, on attachment to Canadian Mine Technology Laboratory, Mining Research Laboratories, CANMET, Energy, Mines and Resources Canada, Ottawa, Ontario.

[2]Physical Scientist, Canadian Mine Technology Laboratory, Mining Research Laboratories, CANMET, Energy, Mines and Resources Canada, Ottawa, Ontario.

COMPORTEMENT POSTRUPTURE DE LA GRANODIORITE DE LAC DU BONNET

par

J.S.O. Lau[1] et B. Gorski[2]

RÉSUMÉ

Un programme d'essais en laboratorie a été mené pour étudier le comportement postrupture de la granodiorite de lac du Bonnet provenant du niveau 420 du LRS. La roche affichait un comportement de classe II. La formation de fissures dans les éprouvettes a semblé commencer à un niveau de contraintes de 35 - 45% de la résistance maximale. La dilatation a commencé à un niveau de contraintes équivalent à environ 65 - 75% de la résistance maximale.

La résistance maximale a augmenté avec la pression de confinement. La résistance à la compression uniaxiale prévue, σ_c, et la constante du matériau, m, dans le critère de rupture de Hoek et Brown pour la granodiorite, étaient respectivement de 224 MPa et de 26.27.

À mesure qu'augmentait la pression de confinement, le mode de rupture allait de fissures et de ruptures conjuguées à une seule rupture de cisaillement ouverte. L'angle d'inclinaison, β, du plan de rupture par rapport à l'axe de l'éprouvette augmentait légèrement avec la pression de confinement comme prévu.

La fermeture des fissures lorsque la pression de confinement a été augmentée de 0 à 10 MPa a causé une augmentation du module tangent d'Young et du coefficient de Poisson. Toutefois, la formation et la croissance des fissures ont donné lieu à une diminution du module d'Young et à une augmentation du coefficient de Poisson au niveau de résistance maximale.

Mots clés: postrupture, uniaxiale, triaxiale, contrainte-déformation, résistance maximale, critère de rupture, angle β, module tangent d'Young, coefficient de Poisson

---

[1]Ingénieur en géotechnique, EACL Recherche, affecté au Laboratoire canadien de technologie minière, Laboratories de recherche minière, CANMET, Énergie, Mines et Ressources Canada, Ottawa, Ontario.

[2]Chercheur en sciences physique, Laboratoire canadien de technologie minière, Laboratoires de recherche minière, CANMET, Énergie, Mines et Ressources Canada, Ottawa, Ontario.

CONTENTS

	Page
ABSTRACT	i
RÉSUMÉ	iii
INTRODUCTION	1
ROCK TYPE AND SPECIMEN PREPARATION	1
TEST APPARATUS AND PROCEDURE	2
TEST PROGRAM AND RESULTS	3
DISCUSSION	4
Stress-Strain Observations	4
Strength and Failure Criterion	5
Failure Mode	6
Tangent Young's Modulus	7
Poisson's Ratio	8
CONCLUSIONS	8
RECOMMENDATIONS	10
ACKNOWLEDGEMENTS	10
REFERENCES	10
APPENDIX A	32

TABLES

No.		
1.	Dimensions, densities and p-wave velocities of rock specimens.	12
2.	Results of post-failure uniaxial and triaxial compression tests.	13
3.	Failure characteristics of rock specimens.	14

FIGURES

1. Stress-strain curves for specimen 401-S12-MB1-36.070 (σ_3 = 0 MPa). . 15
2. Stress-strain curves for specimen 401-S12-MB1-38.207 (σ_3 = 2 MPa). . 16
3. Stress-strain curves for specimen 401-S12-MB1-36.373 (σ_3 = 4 MPa). . 17
4. Stress-strain curves for specimen 401-S12-MB1-36.529 (σ_3 = 6 MPa). . 18
5. Stress-strain curves for specimen 401-S12-MB1-36.687 (σ_3 = 8 MPa). . 19
6. Stress-strain curves for specimen 401-S12-MB1-37.000 (σ_3 = 10 MPa). . 20
7. Stress-strain curves for specimen 401-S12-MB1-37.156 (σ_3 = 15 MPa). . 21
8. Stress-strain curves for specimen 401-S12-MB1-37.343 (σ_3 = 20 MPa). . 22
9. Stress-strain curves for specimen 401-S12-MB1-37.502 (σ_3 = 30 MPa). . 23
10. Stress-strain curves for specimen 401-S12-MB1-37.650 (σ_3 = 40 MPa). . 24
11. Stress-strain curves for specimen 401-S12-MB1-37.805 (σ_3 = 60 MPa). . 25
12. Stress versus axial strain curves of granodiorite in uniaxial and triaxial compression. 26
13. Volumetric strain versus axial strain curves of granodiorite in uniaxial and triaxial compression 27
14. Hoek and Brown failure envelope. 28
15. Plots of angle ϕ versus confining pressure. 29
16. Plots of tangent Young's moduli, E and E_p, versus confining pressure. . 30
17. Plots of Poisson's ratios, ν and ν_p, versus confining pressure. 31

INTRODUCTION

AECL Research is assessing the concept of disposal of high-level nuclear fuel wastes in a vault located 500-1000 m deep in plutonic rock. As part of its program, AECL Research has constructed the Underground Research Laboratory (URL) in the Lac du Bonnet Batholith, near Pinawa, Manitoba, for conducting large-scale geotechnical and hydrogeological investigations. In support of these investigations, the Canada Centre for Mineral and Energy Technology (CANMET), in conjunction with AECL Research, has conducted laboratory-scale studies of rock samples from the URL and the surrounding rocks.

As part of the URL characterization program, studies between 1980 and 1990 focused on determining the mechanical properties in the pre-failure and peak strength regions of the various rock types found at the URL (Annor and Jackson, 1987; Jackson et al., 1989; Lau et al., 1991). More recently, as part of the URL Mine-by experiment, extensive post-failure testing has been carried out on three rock types (grey granite, granodiorite and pink granite) to determine parameters for a brittle elastic-plastic constitutive model developed at the University of Toronto (Ofoegbu and Curran, 1991). Results of post-failure testing on grey granite have been reported in CANMET Division Report MRL 91-079(TR) (Lau and Gorski, 1991). This report presents and discusses the results of the post-failure uniaxial and triaxial tests on the Lac du Bonnet granodiorite.

ROCK TYPE AND SPECIMEN PREPARATION

Samples used in these tests were HQ rock cores obtained from borehole 401-S12-MB1 at the 420 Level of the URL. The rock type is a medium- to coarse-grained granodiorite.

Specimens were prepared in accordance with the procedure described in the Pit Slope Manual Supplement 3-5 (Gyenge and Ladanyi, 1977) and the method suggested by the International Society for Rock Mechanics (Brown, 1981). The end surfaces of each of the specimens were ground flat to 0.025 mm to ensure that they were parallel to each other and perpendicular to the axis of the specimen.

The dimensions and bulk densities of the specimens are listed in Table 1. It should be noted that in Table 1, the last number in the specimen identification represents the downhole depth of the specimen in metres. The mean bulk density of the granodiorite specimens was found to be 2.66 Mg/m^3. Specimen lengths varied from 148.41 to 154.54

mm and diameters varied from 60.74 to 60.90 mm, with length to diameter ratios ranging from 2.44 to 2.54. Table 1 also shows the zero-pressure p-wave velocities measured on the specimens prior to testing. The mean p-wave velocity of the granodiorite was found to be 3.704 km/s. This is slightly higher than that (3.594 km/s) of the grey granite obtained from the same borehole (Lau and Gorski, 1991).

TEST APPARATUS AND PROCEDURE

The post-failure uniaxial and triaxial compression tests were conducted using the MTS 815 Rock Mechanics Test System, which is a computer-controlled, servo-hydraulic compression machine, consisting of a 2.22 MN rated load cell, load frame, hydraulic power supply, triaxial cell, confining pressure subsystem, test controller, test processor and DEC micro PDP 11/73 computer. The triaxial cell is equipped with three linear variable differential transducers (LVDTs) for the measurement of axial deformations and an extensometer with a circumferential kit for the measurement of circumferential deformation. For a detailed description of the MTS system and its operation, the reader is referred to the MTS Operation Manual (MTS Systems Corp., 1986) and CANMET Division Report MRL 87-33(INT) (Gorski, 1987).

The procedures to conduct the post-failure uniaxial and triaxial compression tests were similar, except that in the triaxial test, the confining pressure and the axial stress were first increased from zero, at the same rate of 0.75 MPa/s, until the desired value of confining pressure was attained. The test (uniaxial or triaxial) began under load control. The axial stress was increased at a rate of 0.75 MPa/s until the axial load exceeded the equilibrium load by 60 kN. The control mode was then switched over to an axial strain rate approximating an axial stress rate of 0.75 MPa/s.

During the test, unloading and reloading cycles were also performed at 40-MPa increments of axial stress. Each unloading sequence consisted of reducing the axial stress to a value slightly above the confining pressure. After the axial stress had reached approximately 75% of the estimated peak strength, unloading was switched to the circumferential strain control mode, performed at 0.063-mm increments of circumferential deformation. It should be noted that loading remained under the axial strain control mode.

As the peak strength of the specimen was approached, special care was taken to prevent rapid failure and enable testing to continue into the post-failure region. The MTS system was programmed in such a way that, when a drop in axial load (initial failure) was detected, the system would immediately unload, reducing the axial strain

by 20%. The system then started to reload again, under the axial strain control mode, until another drop in axial load was detected. It should be noted that at this stage of the testing, unloading-reloading cycles were still performed at 0.063-mm increments of circumferential deformation. The process was repeated until the residual strength of the specimen was attained or the uncontrolled failure of the specimen occurred.

Analog signals from the load cell, LVDTs, extensometer and confining pressure subsystem were scanned every 3 seconds during the test, and the data were stored on hard disk in the PDP 11/73 computer. A real time plot of load versus axial displacement was obtained using a Kipp & Zonen pen recorder wired to the test controller. After the test was terminated, the data were transferred to the VAX 750 computer for data storage and analysis. Plots of axial stress versus axial strain and axial stress versus circumferential strain (loading and unloading curves) were obtained from a DEC LVP16 pen plotter connected to the PDP 11/73 computer.

TEST PROGRAM AND RESULTS

Testing for this study took place in January and February, 1991 at Canadian Mine Technology Laboratory, Mining Research Laboratories, CANMET, Energy, Mines and Resources Canada in Ottawa. The program consisted of eleven tests conducted under the unconfined condition and at confining pressures of 2, 4, 6, 8, 10, 15, 20, 30, 40 and 60 MPa. The loading and unloading curves for each test are presented in Appendix A. The envelopes to these loading and unloading curves were plotted using DATAPLOT computer software. A cubic spline fit was used for data analysis which employed a third degree equation model of the form:

$$\sigma = a_0 + a_1\varepsilon + a_2\varepsilon^2 + a_3\varepsilon^3 \qquad (1)$$

where σ = stress

ε = strain

and a_0, a_1, a_2 and a_3 are coefficients

These envelopes, illustrated in Figures 1 to 13, will be referred to as stress-strain curves in this report. Plots of stress versus volumetric strain are also shown in those figures. Volumetric strain was computed by using the following equation:

$$\varepsilon_v = \varepsilon_a + 2\varepsilon_c \tag{2}$$

where ε_v = volumetric strain
ε_a = axial strain
ε_c = circumferential strain

For each specimen, the deviator stress $(\sigma_1 - \sigma_3)_p$, axial strain ε_{ap} and volumetric strain ε_{vp} at peak load, and the deviator stress $(\sigma_1 - \sigma_3)_u$, axial strain ε_{au} and volumetric strain ε_{vu} at the termination of the test were recorded. The tangent Young's modulus E and Poisson's ratio ν were determined from the stress-strain curves at the stress level of $0.5(\sigma_1 - \sigma_3)_p$. The unloading stiffness E_p and Poisson's ratio ν_p of the specimen at peak strength were determined from the unloading curves of the peak load (Appendix A). These values are given in Table 2.

DISCUSSION

STRESS-STRAIN OBSERVATIONS

Figures 1 to 11 show the stress-strain characteristics for the granodiorite under uniaxial compression and triaxial compression. In general, the pre-failure stress-strain (axial strain) curve may be divided into three regions. The first one is characterized by a steadily increasing slope, marking the closure of microcracks in the specimen. This region is more prominent for tests performed at low confining pressures than those performed at high confining pressures, typical for rock samples obtained from the 420 Level of the URL, due to the presence of stress-induced microcracks in those samples. The second (middle) region is nearly linear, approximating linear elastic behaviour. In the third region, the slope decreases, indicating crack formation, crack growth and sliding on existing crack interfaces. Failure of the specimen was taken as the peak of the stress-strain curve. The post-failure behaviour is marked by regions of abrupt drop in stress and regions of more gentle drop, indicating the formation of larger cracks and steeply inclined shear fractures. Abrupt drops are characterized by positive slopes, indicating class II rock behaviour. Failure for class II rock behaviour is self-sustaining (Wawersik and Fairhurst, 1970), which means the elastic strain energy stored in the specimen at peak load is sufficient to maintain fracture propagation until the specimen has lost its load-carrying ability.

The stress-strain curve for the circumferential strain is nearly linear from initial loading to a stress level equivalent to approximately 35 - 45% of the peak deviator stress. The curve then starts to deviate from linear behaviour, suggesting the development of cracks in the specimen. The slope of the curve decreases steadily and the peak of the curve indicates the failure of the specimen. In the post-failure region, the circumferential strain increases rapidly, especially under conditions of low confining pressure, due to the formation of small fractures and possibly spalling in the specimen.

Failure development and the eventual disintegration of the specimen can be illustrated, using the plot of stress versus volumetric strain (Figs. 1-11). In general, the slope of the curve increases from initial loading to a stress level equal to approximately 65 - 75% of the peak deviator stress, where the volumetric strain reaches its maximum value. The only exception is the curve for the test performed under the unconfined condition. The maximum volumetric strain is reached at a higher stress level equivalent to approximately 85% of the peak deviator stress. The discrepancy is due to the larger axial strain recorded at the beginning of the unconfined test. For all tests, the slope of the curve becomes negative after the maximum volumetric strain has been reached, suggesting the formation and growth of cracks in the specimen and the onset of dilation. The maximum rate of cracking occurs at failure at the peak of the curve. In the post-failure region, the volumetric strain increases rapidly as the stress decreases, due to the disintegration of the specimen.

The stress-strain (axial strain) curves and the volumetric strain versus axial strain curves for the entire series of tests are plotted in Figures 12 and 13 respectively to study the effect of the confining pressure on the stress-strain curves. Increase of compressive strength with increasing confining pressure is clearly evident. Progressive increases in post-failure axial strain and reductions in post-failure volumetric strain (dilation) can be observed with increasing confining pressure. It can also be seen that there is a progressive slight flattening of the stress-strain curves with increasing confining pressure.

STRENGTH AND FAILURE CRITERION

The peak strengths of these specimens are taken as the maximum compressive strengths recorded in the tests, and are given as peak deviator stresses in Table 2. From this table and Figure 12, it can be seen that the peak strength increased with confining pressure.

Although these tests were programmed to continue into the post-failure region until the residual strengths were attained, uncontrolled failure occurred in most tests

before the residual strength was obtained. From Table 2 and Figure 12, it appears that the residual strength was approached somewhere near 34 MPa.

The peak strengths were used to estimate the rock mass strength of the granodiorite, using the Hoek and Brown failure criterion (Hoek and Brown, 1980) which is defined by the following equation:

$$\sigma_1 = \sigma_3 + \sqrt{m\sigma_c\sigma_3 + s{\sigma_c}^2} \tag{3}$$

where σ_1 = major principal stress at failure
σ_3 = minor principal stress applied to the rock sample
σ_c = uniaxial compressive strength of the intact rock material in the specimen
m and s are constants and for these intact rock specimens, $s = 1$

The predicted uniaxial compressive strength of the intact rock material, σ_c, and the material constant, m, for the granodiorite were calculated using the equations suggested by Hoek and Brown (1980), and found to be 224 MPa and 26.27 respectively. The failure envelope developed using these values of σ_c and m and Equation 3 is shown in Figure 14. Compared with the grey granite (σ_c = 157 MPa, m = 35.28) obtained from the same borehole (Lau and Gorski, 1991), the granodiorite is a stronger rock.

FAILURE MODE

The failure characteristics of the specimens are shown in Table 3. Under uniaxial compression and conditions of low confining pressure (2 - 10 MPa), cracks and low angle conjugate fractures developed in the specimens. Only a few axial cracks were observed in the specimen under uniaxial compression. This might explain why the granodiorite had a considerably higher uniaxial compressive strength than the grey granite. Multiple axial cracks developed in the grey granite specimens under uniaxial compression (Lau and Gorski, 1991), resulted in lower compressive strength at failure due to the disintegration of the specimens. Under conditions of higher confining pressure (15 - 60 MPa), cracks and single open shear fractures developed in the granodiorite specimens, occasional with splays.

For each specimen, the inclination angle, β, of the fracture plane with the specimen axis was measured and is shown in Table 3. The angle β was found to increase

slightly with increasing confining pressure. These angles are plotted against confining pressure in Figure 15. Also plotted as a solid line is the relationship between fracture plane inclination and confining pressure calculated by means of the following equations suggested by Hoek and Brown (Hoek and Brown, 1980), using σ_c = 224 MPa and m = 26.27:

$$\tau_m = \frac{1}{2}(\sigma_1 - \sigma_3) \tag{4}$$

$$\sigma = \sigma_3 + \frac{\tau_m^2}{\tau_m + m\sigma_c/8} \tag{5}$$

$$\tau = (\sigma - \sigma_3)\sqrt{1 + m\sigma_c/4\tau_m} \tag{6}$$

The angle β is defined by:

$$sin2\beta = \frac{\tau}{\tau_m} \tag{7}$$

There is a general agreement between the measured and predicted values of angle β. This suggests that Equation 7 can be used to give a rough guide to the inclination of shear fractures in the granodiorite.

TANGENT YOUNG'S MODULUS

The tangent Young's modulus, E, for each of the specimens was computed from the stress-strain curve at the stress level equal to 50% of the peak deviator stress, $0.5(\sigma_1 - \sigma_3)_p$. The value of E was determined by substituting the axial strain value at $0.5(\sigma_1 - \sigma_3)_p$ into the derivative of the best-fit equation (Eq. 1) representing the stress-strain curve (Figs. 1-11). Similarly, for each specimen, the unloading stiffness at peak strength, E_p, was also determined from the unloading curve of the peak load (Appendix A). These values are given in Table 2 and are plotted against confining pressure in Figure 16.

Figure 16 reveals the effect of confining pressure on the tangent modulus E. The modulus increased as the confining pressure increased from 0 to 10 MPa, suggesting that some stress relaxation had occurred in these specimens, resulting in higher crack porosities, larger deformations and lower modulus values at low confining pressures. Above 10 MPa, the confining pressure had little effect on the modulus E.

Confining pressure appeared to have little effect on the unloading stiffness at peak strength, E_p. The values of E_p were found to be lower than those of E under triaxial compression. The reduction in stiffness at peak strength was a result of crack development and crack growth in the specimens. Under uniaxial compression, the value of E_p was found to be higher than that of E. Similar behaviour was observed in the post-failure tests of the grey granite (Lau and Gorski, 1991). It appears that under uniaxial compression, cyclic loading in the pre-failure region had some stiffening effect on the specimen in the axial direction.

POISSON'S RATIO

The Poisson's ratio, ν, for each of the specimens was determined from the ratio of the circumferential to the axial tangent moduli obtained from the stress-strain curves (Figs. 1-11) at the stress level equivalent to $0.5(\sigma_1 - \sigma_3)_p$. Similarly, for each specimen, the unloading Poisson's ratio at peak strength, ν_p, was determined from the unloading curves of the peak load. These values are presented in Table 2 and plotted versus confining pressure in Figure 17.

Figure 17 shows that there was a sharp rise in ν when the confining pressure was raised from 0 to 2 MPa, followed by a more gradual increase, indicating the presence of microcracks in these specimens. Above 10 MPa, the confining pressure had no effect on ν. The values of ν_p were found to be considerably higher than those of ν, suggesting that the rate of cracking at peak strength was much higher than that at $0.5(\sigma_1 - \sigma_3)_p$.

CONCLUSIONS

The results of these tests have provided some stress and strain data in the pre-failure, peak strength and post-failure regions of the stress-strain curves for the development of an elastic-brittle-ductile constitutive model for the Lac du Bonnet granodiorite. They have also provided some insight into the post-failure behaviour of the granodiorite which exhibited class II behaviour. This implies that if the behaviour of the granodiorite in the laboratory can be applied directly to its behaviour in the field, in situ fracturing

in the granodiorite could proceed unstably with the release of considerable amount of strain energy and violent failure might occur, should the peak strength be exceeded. From the results, the following conclusions can be made.

The stress-strain (axial) curves from initial loading to peak strength are marked progressively by regions of increasing slope, approximate linear elasticity and decreasing slope. The post-failure regions are characterized by series of abrupt and gentle drops in stress. The development of cracks in the specimens appeared to start at stress levels equivalent to approximately 35 - 45% of the peak deviator stresses. The change in the direction of the slope of the stress-strain (volumetric) suggests the onset of dilation at approximately 65 - 75% of the peak deviator stress. The maximum rate of cracking occurred at peak strength. Growth of cracks was also indicated by the reduction in stiffness and increase of Poisson's ratio at peak strength. In the post-failure regions, the circumferential and volumetric strains increased rapidly, suggesting the disintegration of the specimens. Progressive increases in the axial strain and decreases in the circumferential strain and volumetric strain (dilation) with increasing confining pressure were also observed in the post-failure regions.

The peak strength of the granodiorite increased with increasing confining pressure. A failure envelope was developed by using the Hoek and Brown failure criterion. The predicted uniaxial compressive strength, σ_c and the material constant, m, in the failure criterion were calculated and found to be 224 MPa and 26.27 respectively.

Cracks and low angle conjugate fractures developed in the specimens under conditions of low confining pressure (0 - 10 MPa), whereas, single open shear fractures and cracks formed under conditions of high confining pressure (15 - 60 MPa). The fracture plane inclination (angle β) increased slightly with increasing confining pressure. There is a general agreement between the measured and predicted values of angle β.

The tangent Young's modulus E increased with increasing confining pressure from 0 to 10 MPa, indicating the presence of microcracks in these specimens. Above 10 MPa, the confining pressure had little effect on the modulus. The confining pressure also appeared to have little effect on the unloading stiffness at peak strength, E_p. However, the values of E_p were found to be lower than those of E under triaxial compression. The reduction in stiffness at peak strength was a result of crack development and growth.

The Poisson's ratio ν increased when the confining pressure was raised from 0 to 10 MPa. Above that, the confining pressure had no effect on the Poisson's ratio. The values of the Poisson's ratio at peak strength, ν_p, were found to be considerably higher than those of ν, indicating the rate of cracking at peak strength was much higher than that at 50% of the peak strength.

RECOMMENDATIONS

One of the main rock mechanics issues related to the construction and operation of the URL is experimentally identifying the pre-failure, peak strength and post-failure behaviours of the host rock. This post-failure uniaxial and triaxial compression testing program has addressed this issue and is recommended for the URL characterization program and Mine-by experiment, and for any future site selection and repository design programs if the disposal concept is deemed acceptable.

Although the granodiorite was observed to exhibit class II behaviour in the laboratory, it should be noted that recent studies by other investigators have shown that class II behaviour observed in testing of rock may be a scale effect rather than a property of the rock (Labuz and Biolzi, 1991). A program to study the scale effect in post-failure testing is therefore strongly recommended for the Mine-by experiment.

From the results of these tests, it is still not clear what the residual strength of the rock is. The problem is the uncontrolled failure of the specimen often occurred before the residual strength was reached. Further research on experimental technique is required to prevent premature failure before the residual strength is reached.

ACKNOWLEDGEMENTS

The authors wish to express their thanks to R. Jackson of CANMET for reviewing this report and making several helpful suggestions. Gratitude is expressed to J. Folta of CANMET for the preparation of specimens and for carrying out the compression wave velocity measurements on the specimens.

REFERENCES

Annor, A. and Jackson, R. (1987), "Mechanical, thermomechanical and joint properties of rock samples from the Lac du Bonnet Batholith, Manitoba" in Geotechnical studies at Whiteshell Research Area (RA-3) (edited by Katsube, T.J. and Hume, J.P.), Divisional Report MRL 87-52(TR), CANMET, Energy, Mines and Resources Canada, p. 49-110.

Brown, E.T. (1981), "Rock characterization testing and monitoring, ISRM suggested methods", International Society for Rock Mechanics, the Commission on Testing Methods, Pergamon, 211 p.

Gorski, B. (1987), "Post-failure uniaxial strength determinations using a servo-hydraulic test system", Division Report MRL 87-33(INT), CANMET, Energy, Mines and Resources Canada, 77 p.

Gyenge, M. and Ladanyi, B. (1977), "Pit slope manual supplement 3-5 - sampling and specimen preparation", CANMET, Report 77-29, 30 p.

Hoek, E. and Brown, E.T. (1980), "Underground excavations in rock", The Institution of Mining and Metallurgy, London, 527 p.

Jackson, R., Lau, J.S.O. and Annor, A. (1989), "Mechanical, thermo-mechanical and joint properties of rock samples from the site of AECL's Underground Research Laboratory, Lac du Bonnet, Manitoba", in Proceedings of the 42nd Canadian Geotechnical Conference, Winnipeg, Manitoba, October 23-25, 1989, p. 41-49.

Labuz, J.F. and Biolzi, L. (1991), "Class I vs class II stability: a demonstration of size effect", Int. J. Rock Mech. Min. Sci. & Geomech. Abstr. Vol. 28, No. 2/3, p. 199-205.

Lau, J.S.O. and Gorski, B. (1991), "The post-failure behaviour of the Lac du Bonnet grey granite", Divisional Report MRL 91-079(TR), CANMET, Energy, Mines and Resources Canada, 140 p.

Lau, J.S.O., Jackson, R. and Gorski, B. (1991), "The effects of temperature and pressure on the mechanical properties of Lac du Bonnet grey granite", in Proceedings of the 32nd U.S. Symposium on Rock Mechanics, Norman, Oklahoma, July 10-12, 1991, p. 313-323.

MTS Systems Corporation (1986), "Operation manual for 815 rock mechanics test systems", MTS Systems Corp., Minneapolis, Minnesota, U.S.A.

Ofoegbu, G.I. and Curran, J.H. (1991), "Development and numerical implementation of an elastic-brittle-ductile constitutive model for intact rock", Department of Civil Engineering, University of Toronto, Publication 91-01, 106 p.

Wawersik, W.R. and Fairhurst, C. (1970), "A study of brittle rock fracture in laboratory compression experiments", Int. J. Rock Mech. Min. Sci., Vol. 7, p. 561-575.

Table 1. Dimensions, densities and p-wave velocities of rock specimens.

Specimen identification	Length (mm)	Diameter (mm)	Bulk density (Mg/m^3)	P-wave velocity (km/s)
401-S12-MB1-36.070	148.41	60.76	2.67	3.875
401-S12-MB1-36.373	151.07	60.86	2.67	3.489
401-S12-MB1-36.529	154.33	60.90	2.66	3.746
401-S12-MB1-36.687	150.14	60.74	2.67	3.680
401-S12-MB1-37.000	151.41	60.77	2.66	3.785
401-S12-MB1-37.156	151.88	60.80	2.66	3.741
401-S12-MB1-37.343	153.24	60.84	2.65	3.657
401-S12-MB1-37.502	149.36	60.82	2.66	3.697
401-S12-MB1-37.650	152.59	60.89	2.66	3.758
401-S12-MB1-37.805	153.71	60.79	2.66	3.805
401-S12-MB1-38.207	154.54	60.82	2.65	3.512
Mean			2.66	3.704
Standard deviation			0.01	0.117

Table 2. Results of post-failure uniaxial and triaxial compression tests.

Specimen Identification	σ_3	Deviator Stress		Axial Strain		Volumetric Strain		Young's Modulus		Poisson's Ratio	
		$(\sigma_1 - \sigma_3)_p$	$(\sigma_1 - \sigma_3)_u$	ε_{ap}	ε_{au}	ε_{vp}	ε_{vu}	E	E_p	ν	ν_p
	(MPa)	(MPa)	(MPa)	(10^{-2})	(10^{-2})	(10^{-2})	(10^{-2})	(GPa)	(GPa)		
401-S12-MB1-36.070	0	198	71	0.467	0.460	0.076	-4.616	56.68	60.41	0.20	0.33
401-S12-MB1-38.207	2	228	34	0.530	0.625	-0.225	-1.986	59.12	59.57	0.30	0.76
401-S12-MB1-36.373	4	255	64	0.569	0.658	-0.314	-2.055	61.19	59.42	0.32	0.85
401-S12-MB1-36.529	6	282	65	0.617	0.707	-0.561	-1.624	63.07	57.61	0.30	1.09
401-S12-MB1-36.687	8	303	103	0.653	0.699	-0.743	-1.762	63.71	57.06	0.35	1.21
401-S12-MB1-37.000	10	327	307	0.646	0.627	-0.564	-0.693	67.39	58.29	0.34	1.06
401-S12-MB1-37.156	15	390	388	0.726	0.734	-0.472	-0.581	65.78	60.42	0.35	0.93
401-S12-MB1-37.343	20	438	400	0.833	0.792	-0.629	-0.755	64.89	59.12	0.35	0.96
401-S12-MB1-37.502	30	500	497	0.899	0.899	-0.413	-0.446	65.31	61.07	0.36	0.78
401-S12-MB1-37.650	40	537	282	0.977	0.958	-0.472	-0.699	64.98	61.10	0.34	0.75
401-S12-MB1-37.805	60	616	375	1.049	0.902	-0.036	-0.388	65.01	64.59	0.34	0.54

Table 3. Failure Characteristics of rock specimens.

Specimen Identification	σ_3 (MPa)	β (degree)	Failure Characteristics
401-S12-MB1-36.070	0	10	conjugate fractures, cracks
401-S12-MB1-38.207	2	13	conjugate fractures, cracks
401-S12-MB1-36.373	4	15	conjugate fractures, cracks
401-S12-MB1-36.529	6	15	conjugate fractures, cracks
401-S12-MB1-36.687	8	15	conjugate fractures, cracks
401-S12-MB1-37.000	10	15	conjugate fractures, cracks
401-S12-MB1-37.156	15	15	shear fracture, cracks
401-S12-MB1-37.343	20	18	shear fracture, cracks
401-S12-MB1-37.502	30	20	shear fracture, cracks
401-S12-MB1-37.650	40	23	shear fracture, splays, cracks
401-S12-MB1-37.805	60	23	shear fracture, cracks

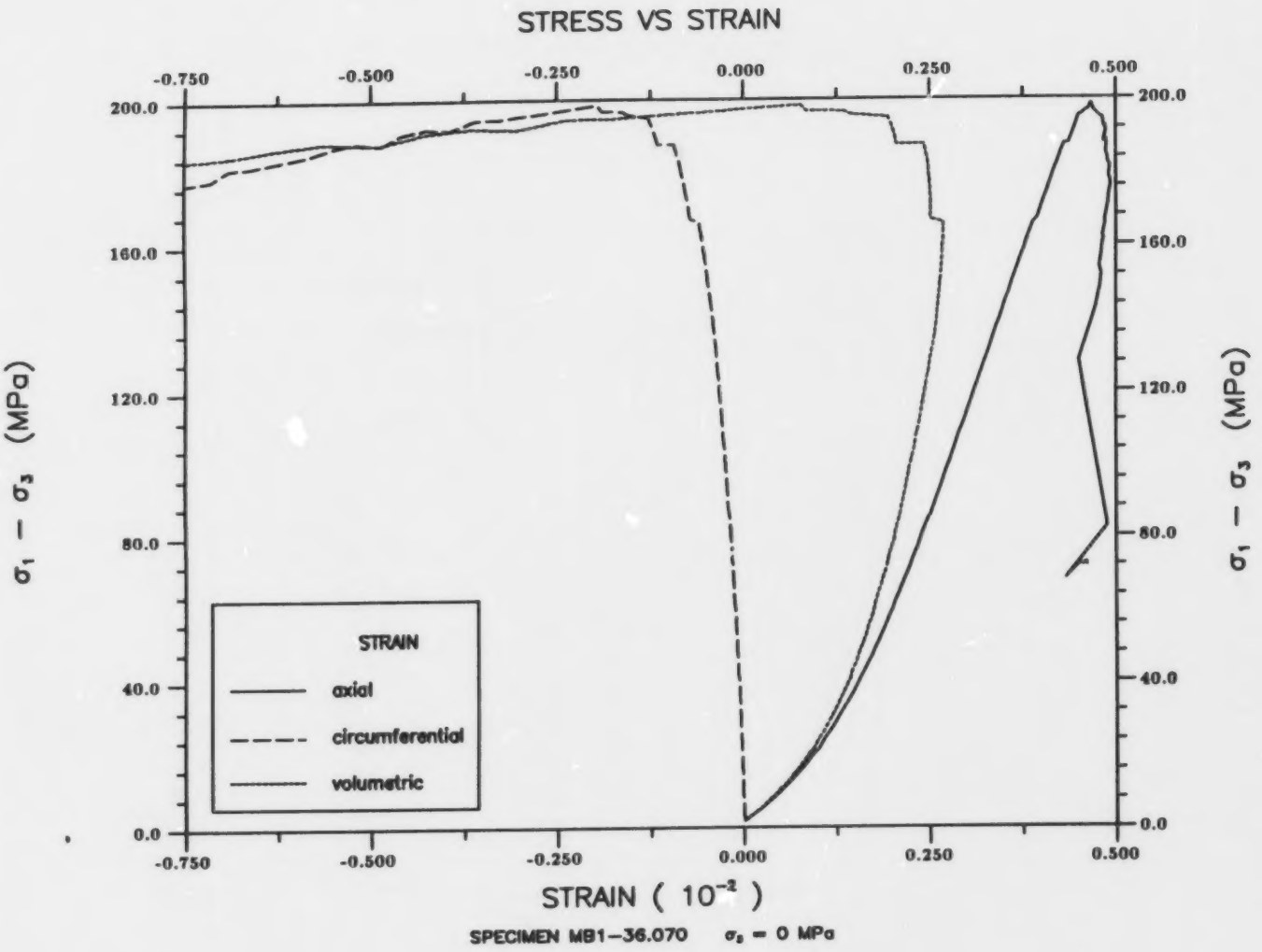

Figure 1. Stress-strain curves for specimen 401-S12-MB1-36.070 ($\sigma_3 = 0$).

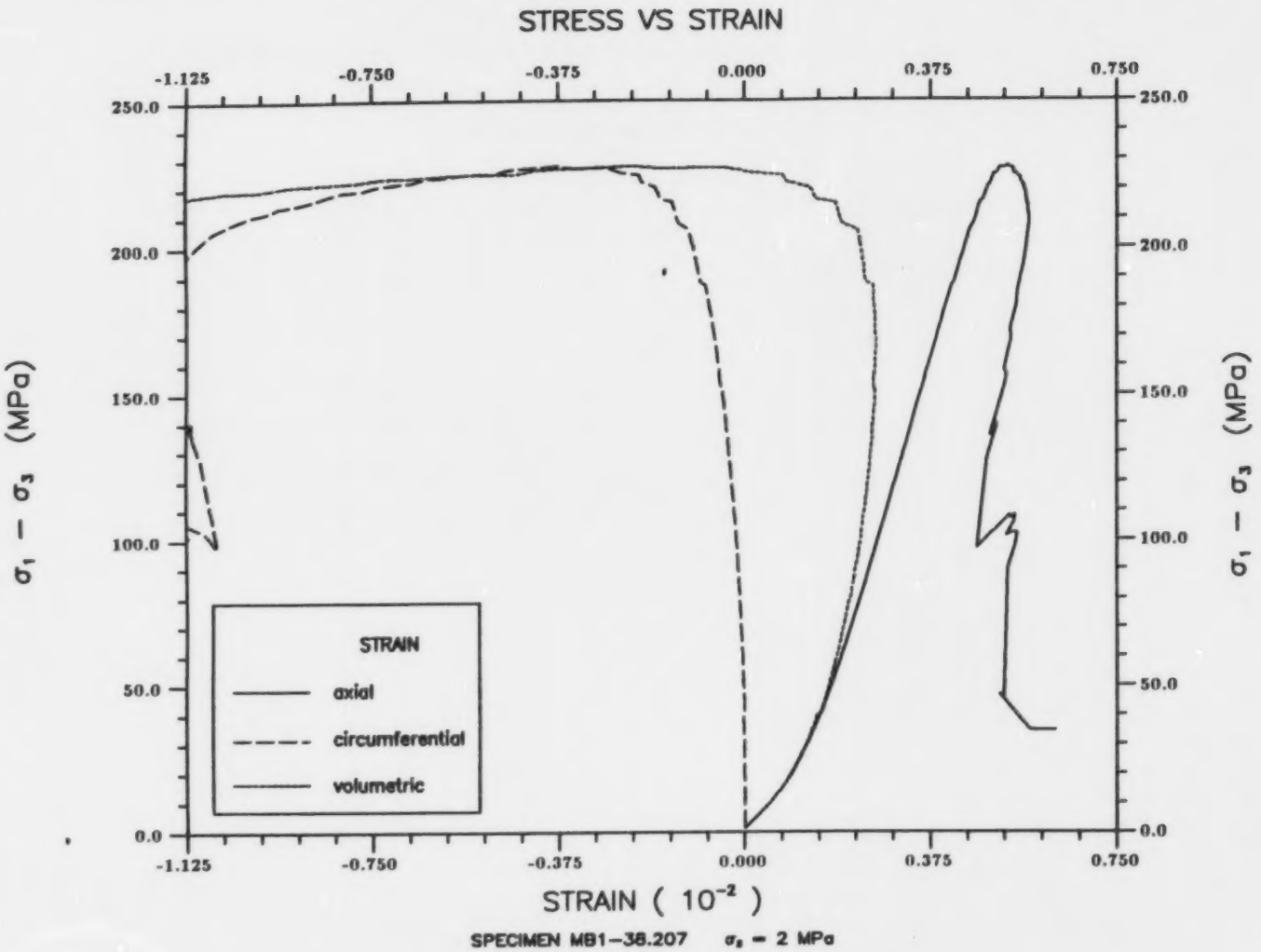

Figure 2. Stress-strain curves for specimen 401-S12-MB1-38.207 ($\sigma_3 = 2$ MPa).

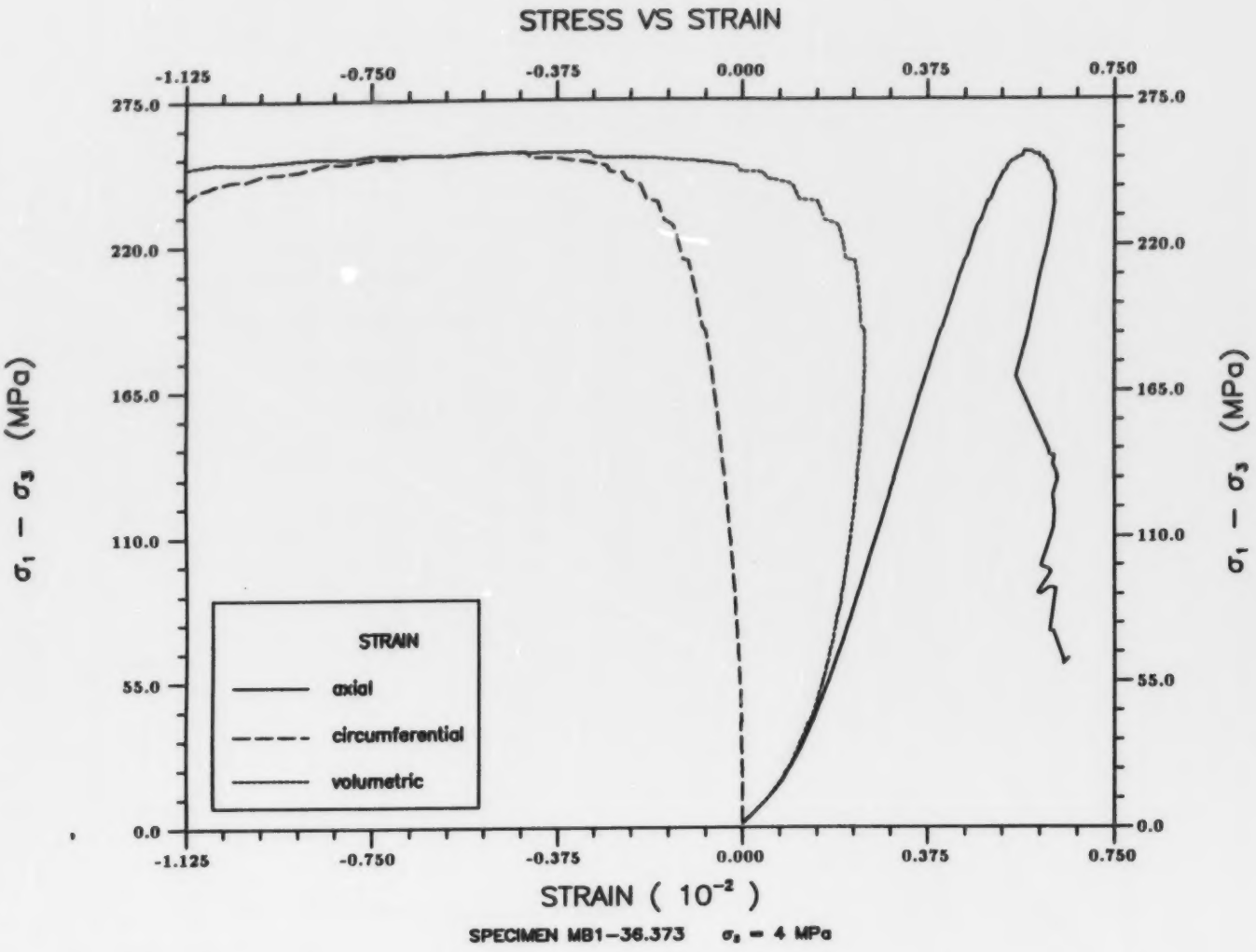

Figure 3. Stress-strain curves for specimen 401-S12-MB1-36.373 ($\sigma_3 = 4$ MPa).

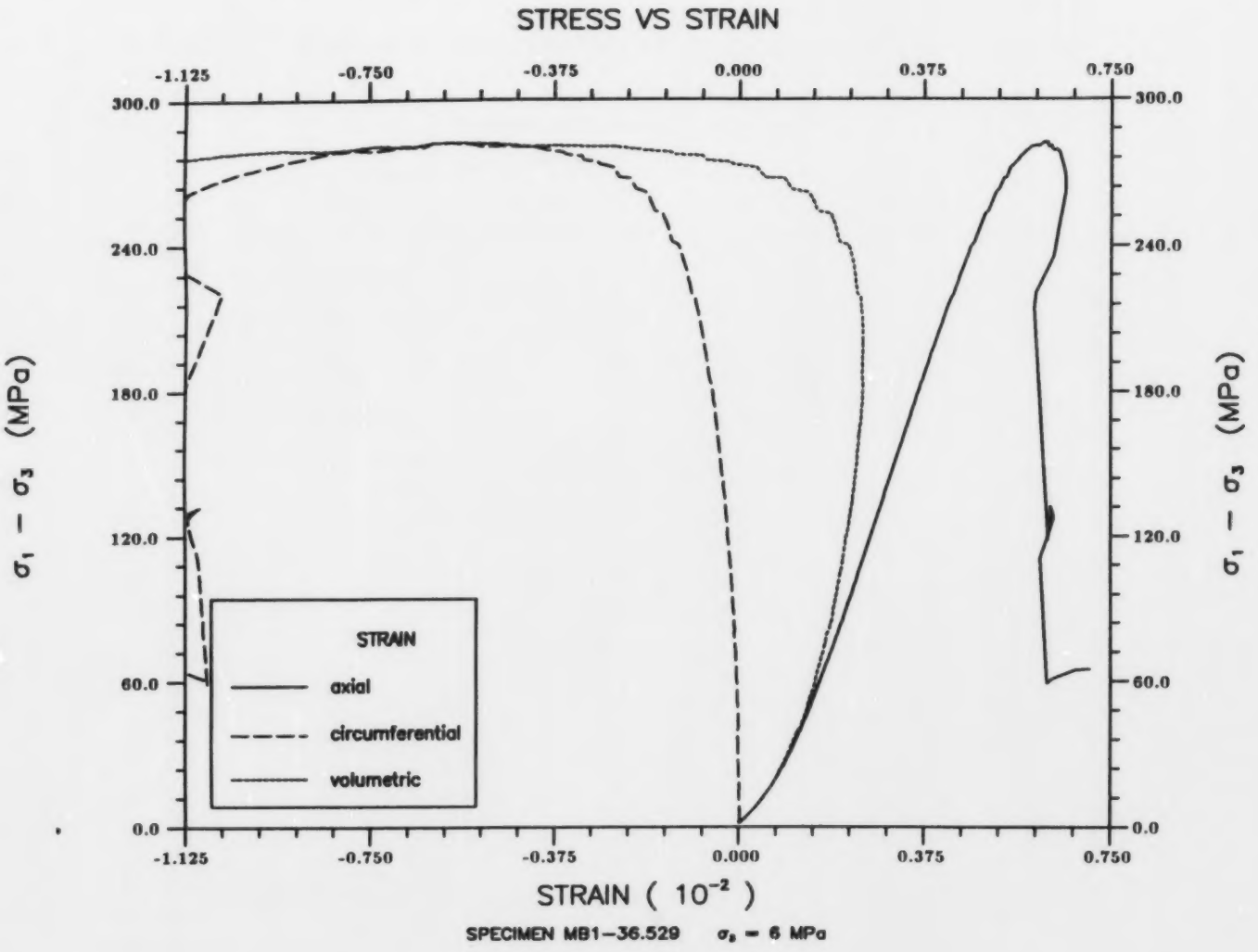

Figure 4. Stress-strain curves for specimen 401-S12-MB1-36.529 ($\sigma_3 = 6$ MPa).

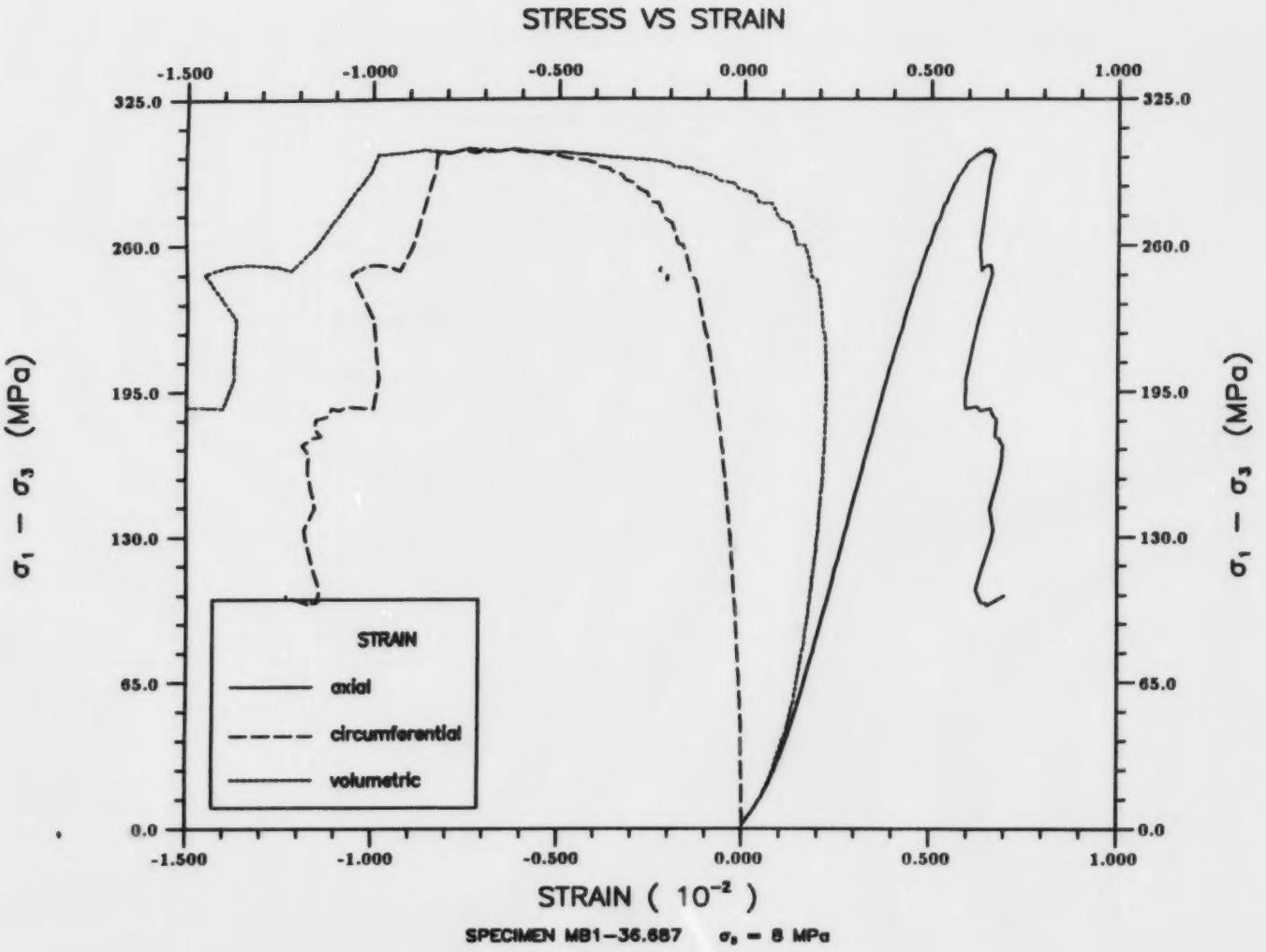

Figure 5. Stress-strain curves for specimen 401-S12-MB1-36.687 ($\sigma_3 = 8$ MPa).

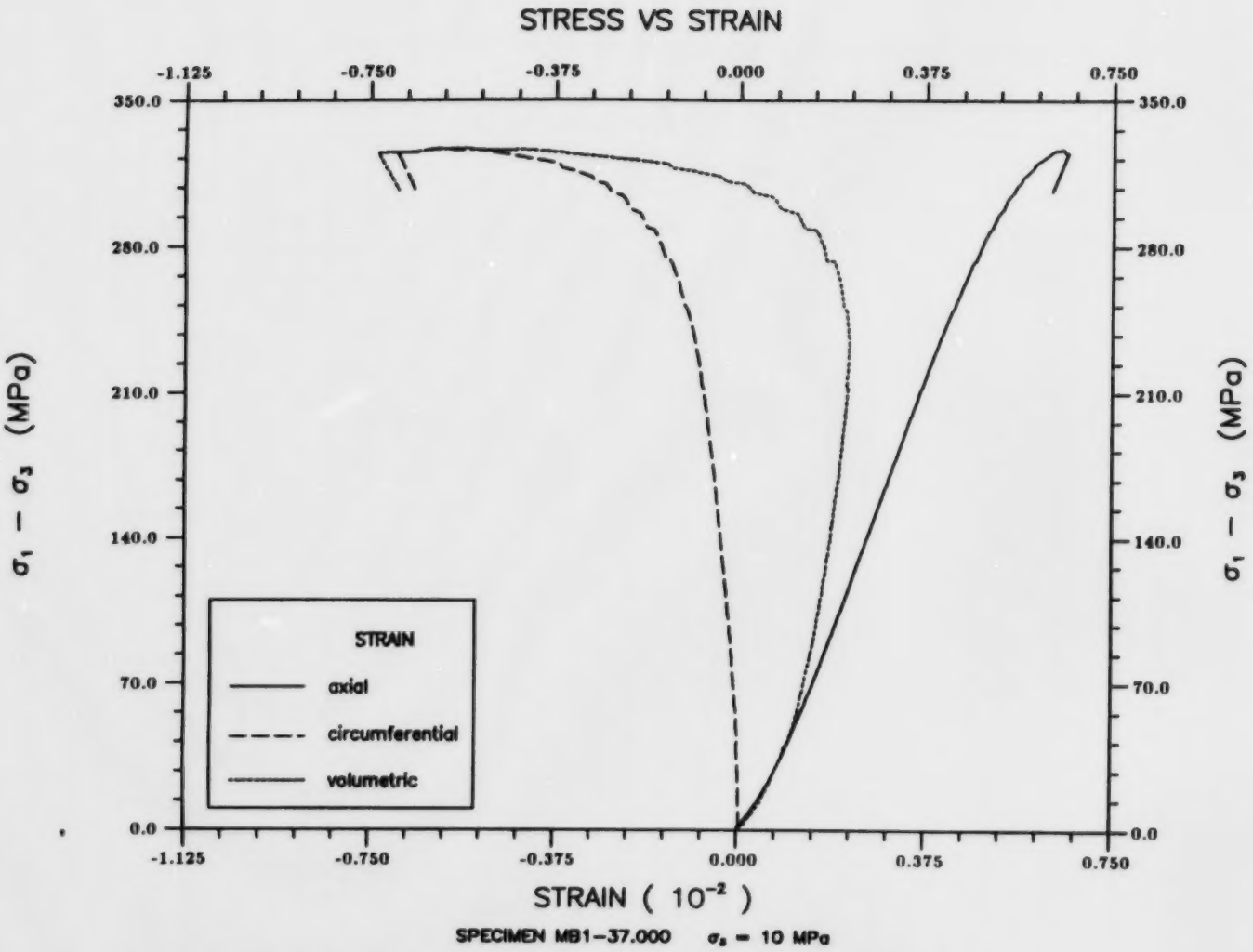

Figure 6. Stress-strain curves for specimen 401-S12-MB1-37.000 ($\sigma_3 = 10$ MPa).

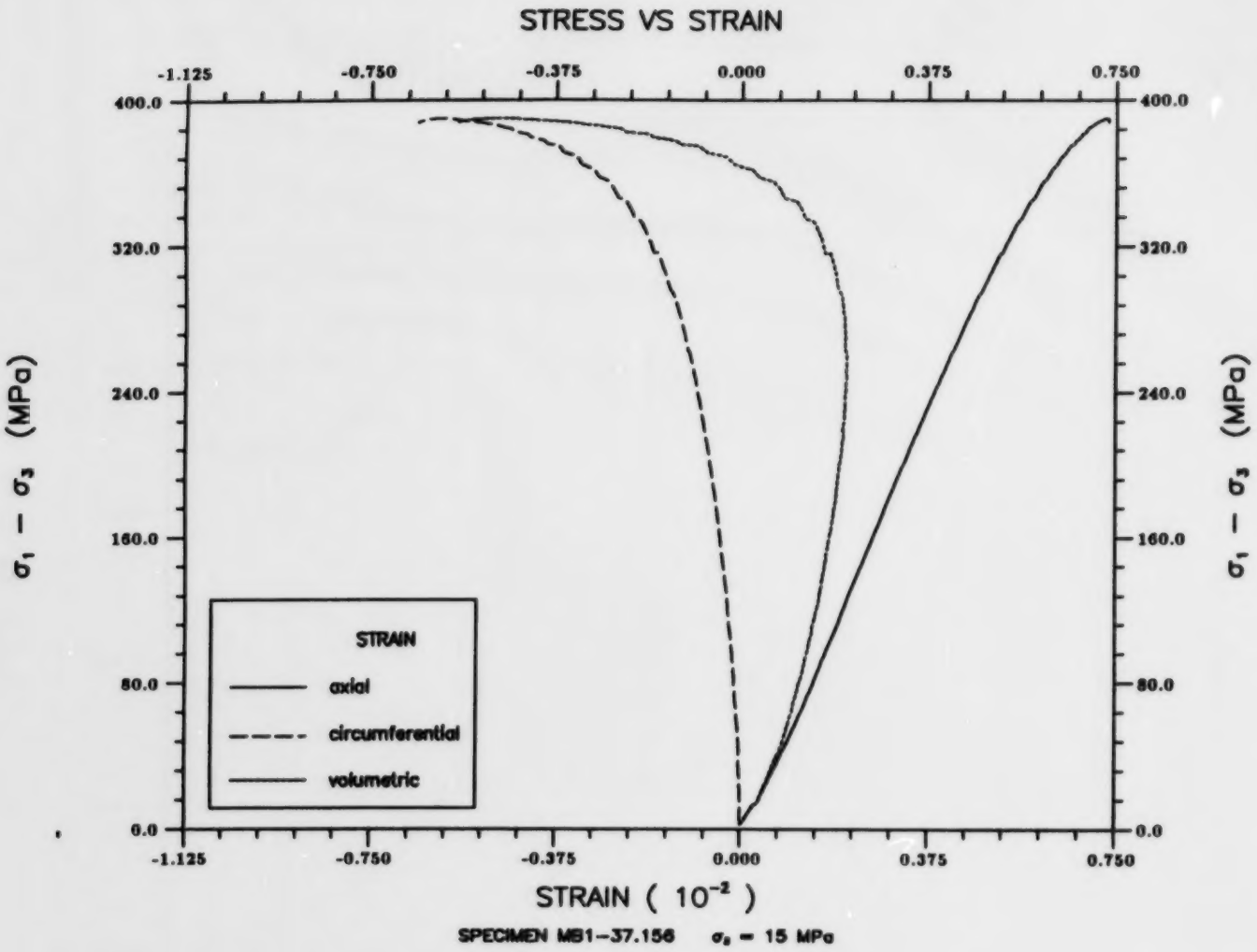

Figure 7. Stress-strain curves for specimen 401-S12-MB1-37.156 ($\sigma_3 = 15$ MPa).

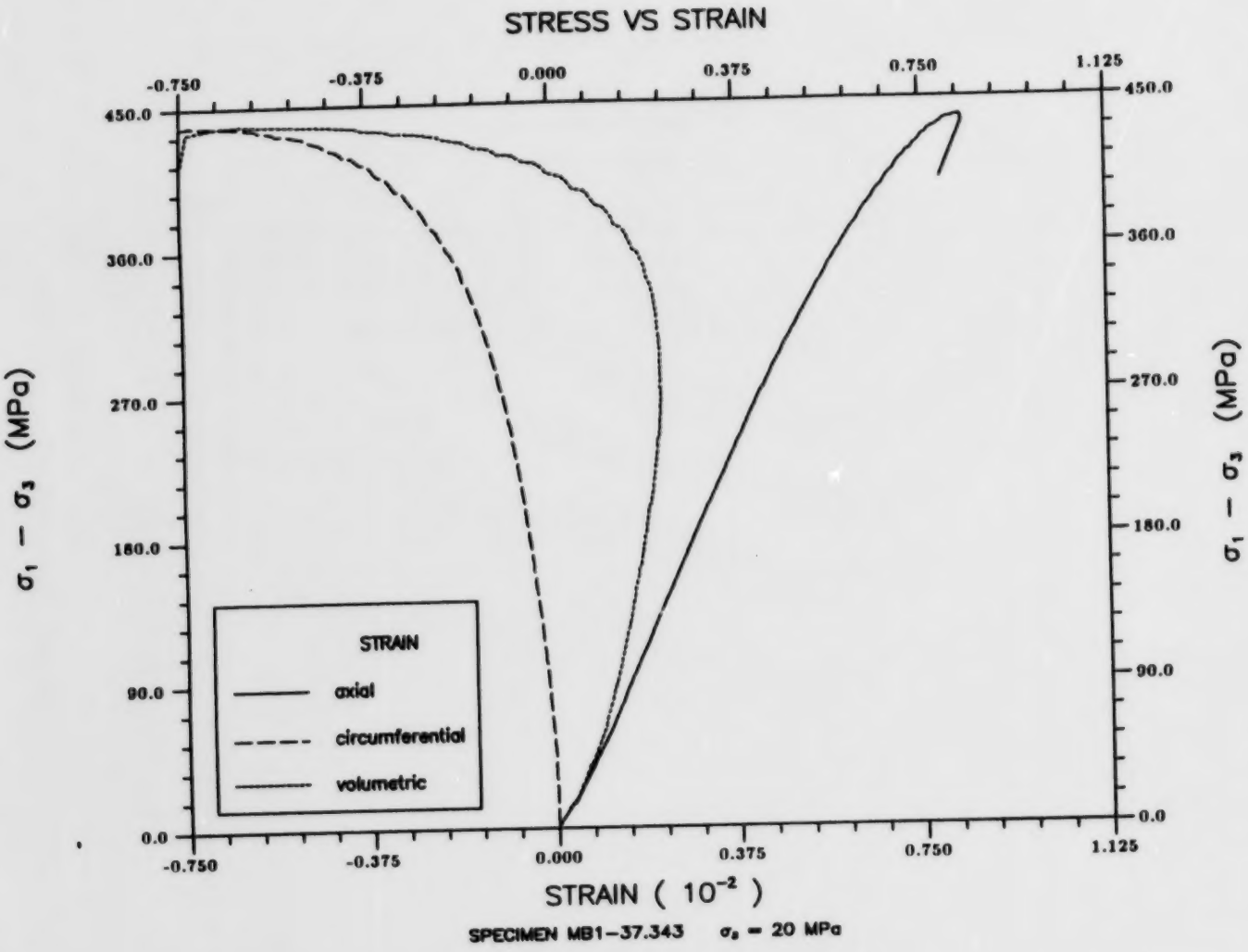

Figure 8. Stress-strain curves for specimen 401-S12-MB1-37.343 ($\sigma_3 = 20$ MPa).

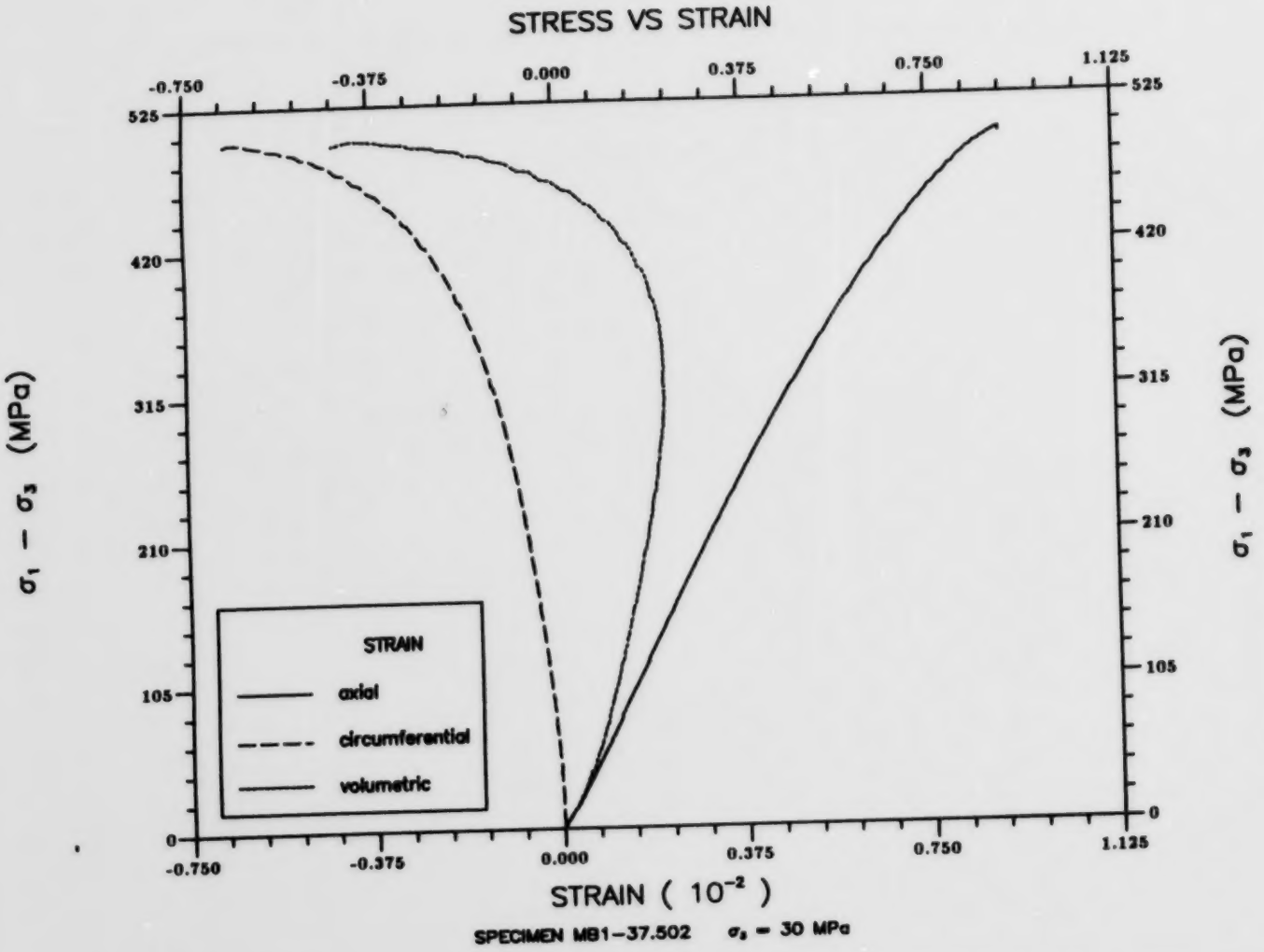

Figure 9. Stress-strain curves for specimen 401-S12-MB1-37.502 (σ_3 = 30 MPa).

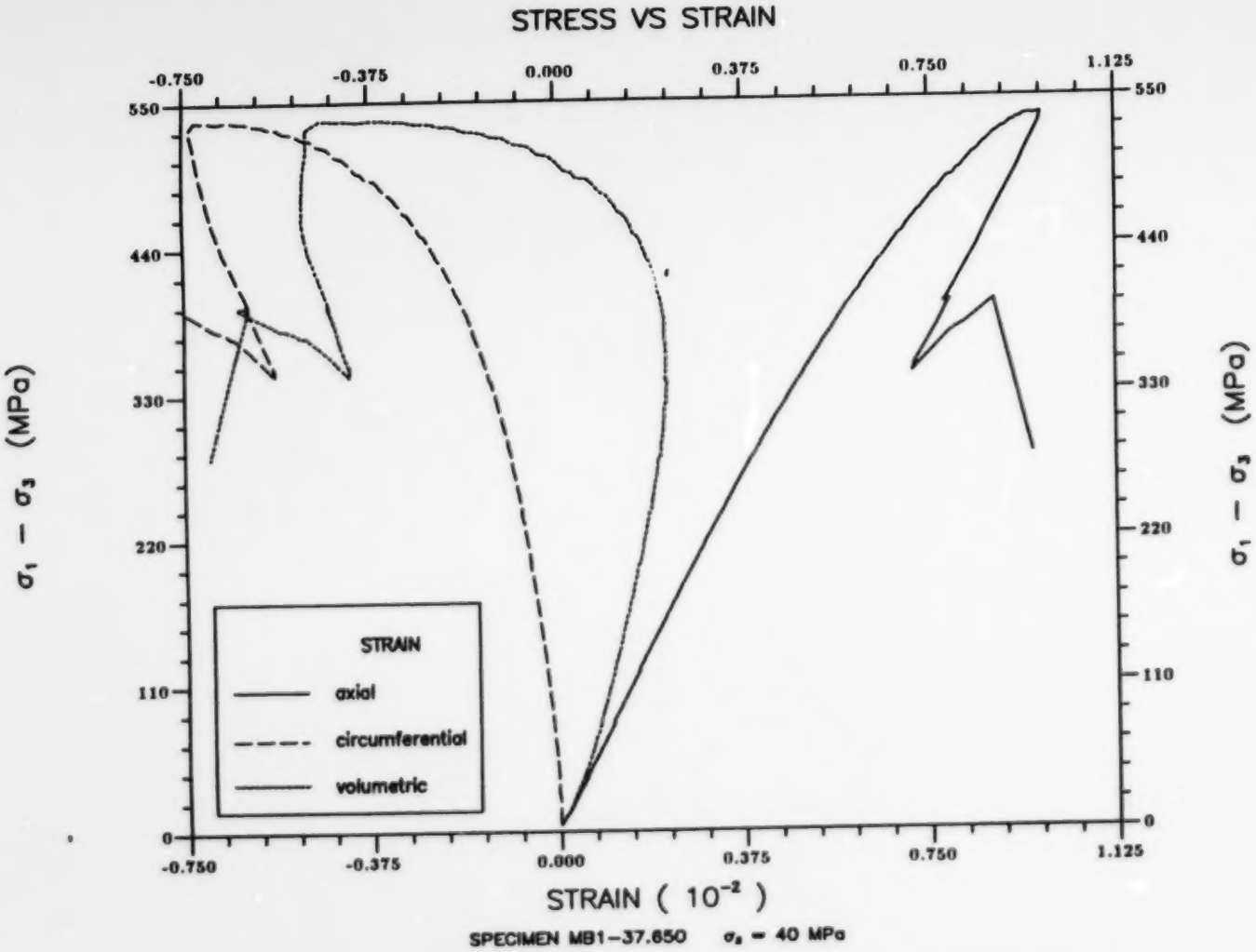

Figure 10. Stress-strain curves for specimen 401-S12-MB1-37.650 (σ_3 = 40 MPa).

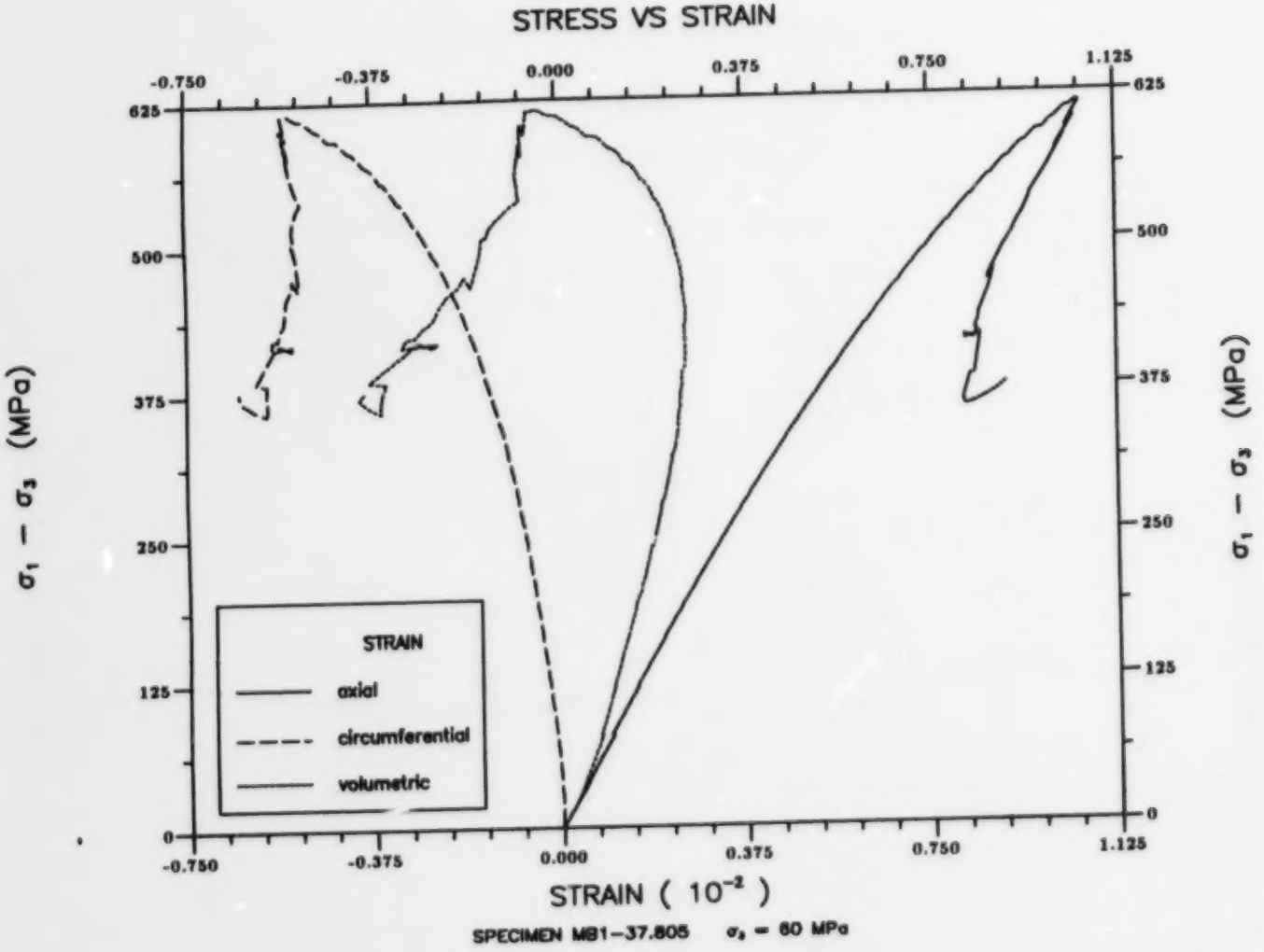

Figure 11. Stress-strain curves for specimen 401-S12-MB1-37.805 (σ_3 = 60 MPa).

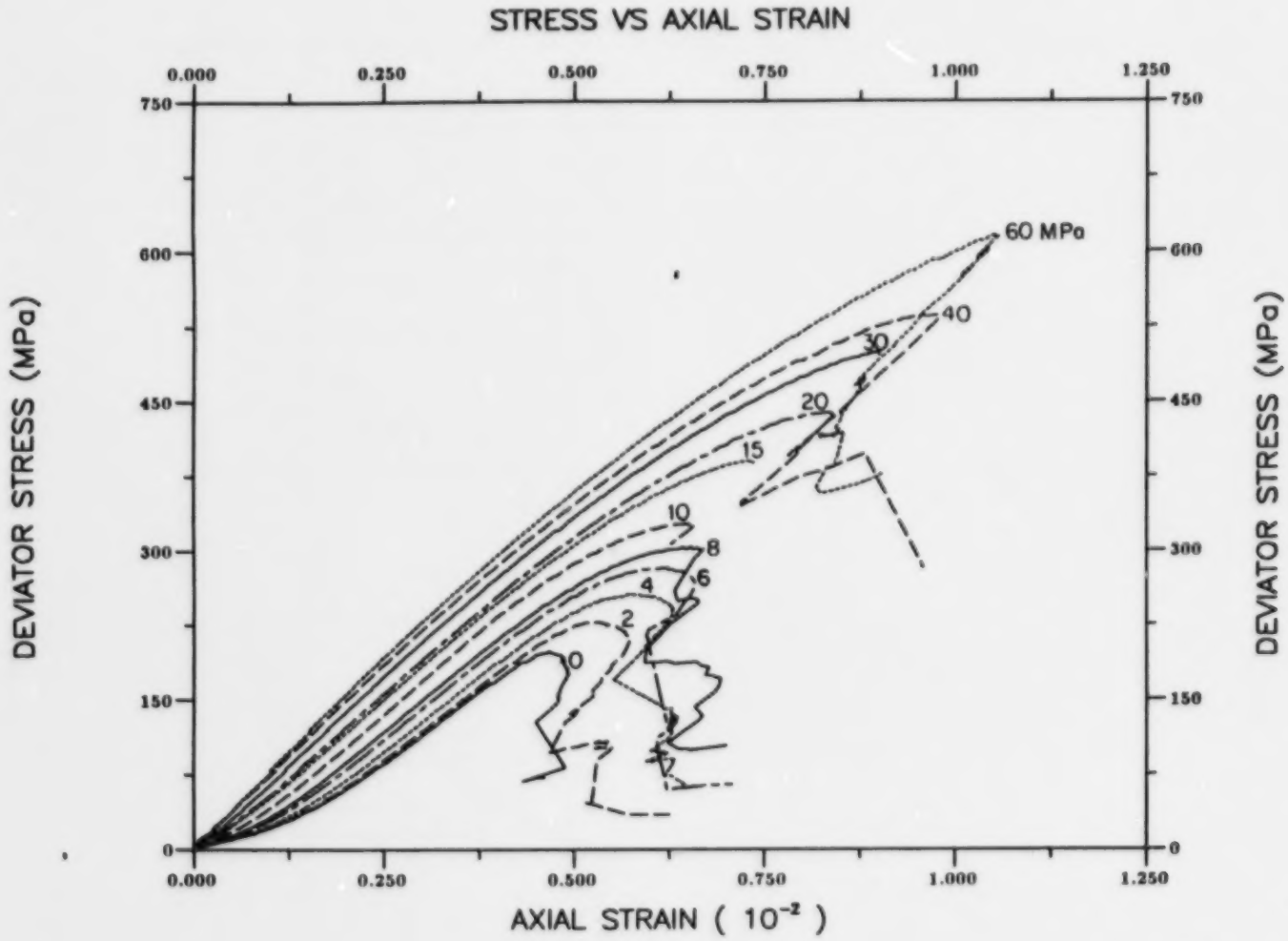

Figure 12. Stress versus axial strain curves of granodiorite in uniaxial and triaxial compression.

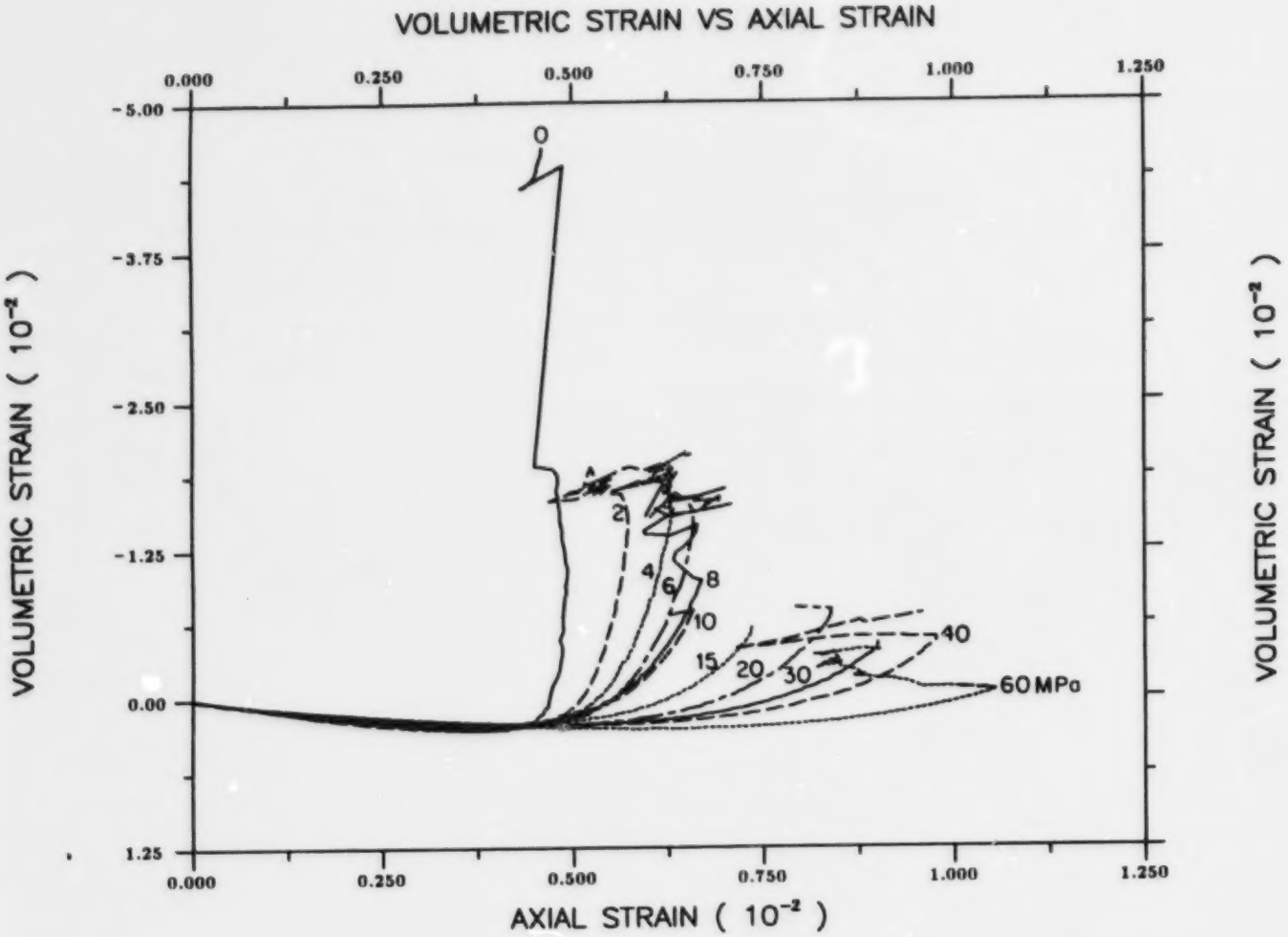

Figure 13. Volumetric strain versus axial strain curves of granodiorite in uniaxial and triaxial compression.

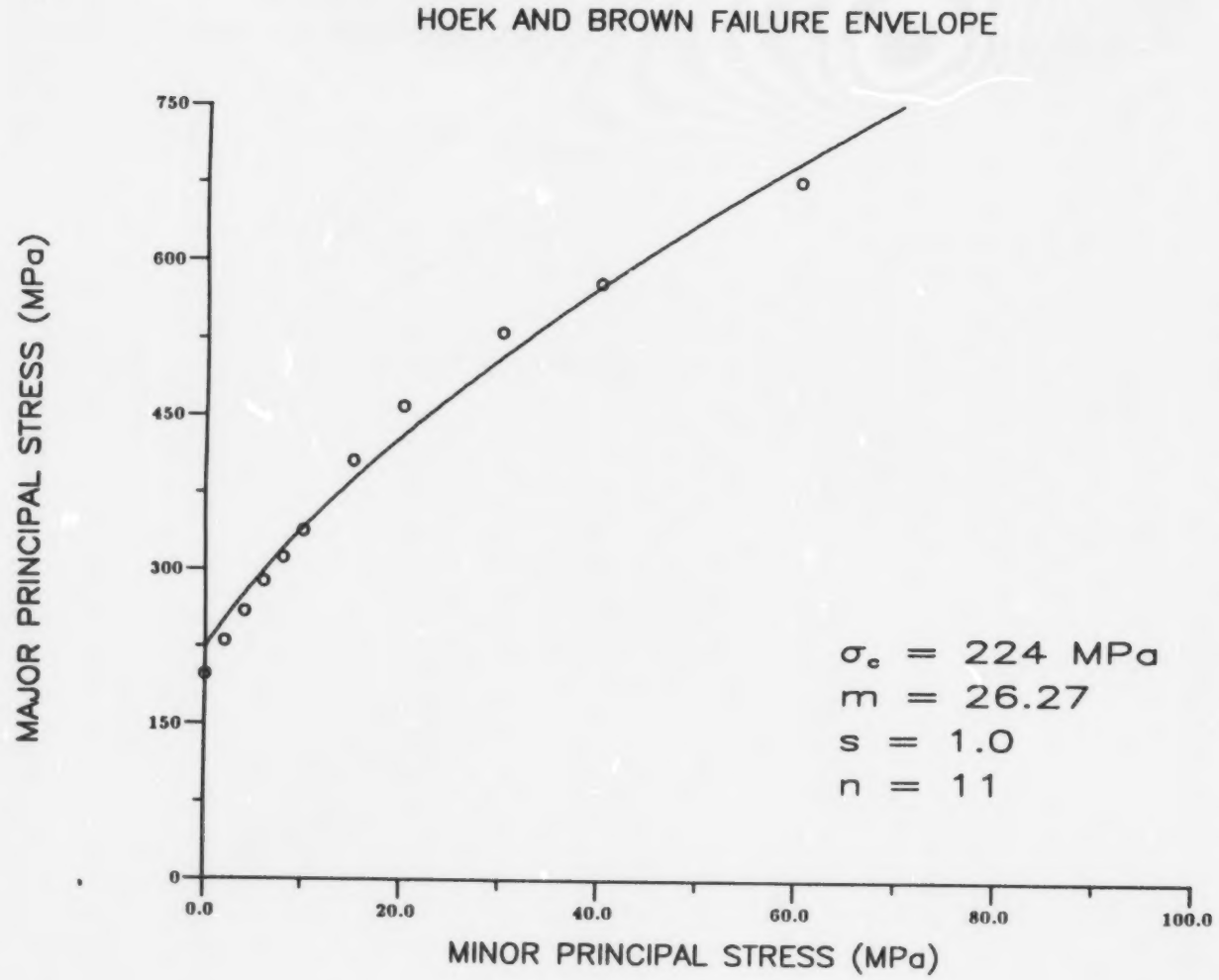

Figure 14. Hoek and Brown failure envelope.

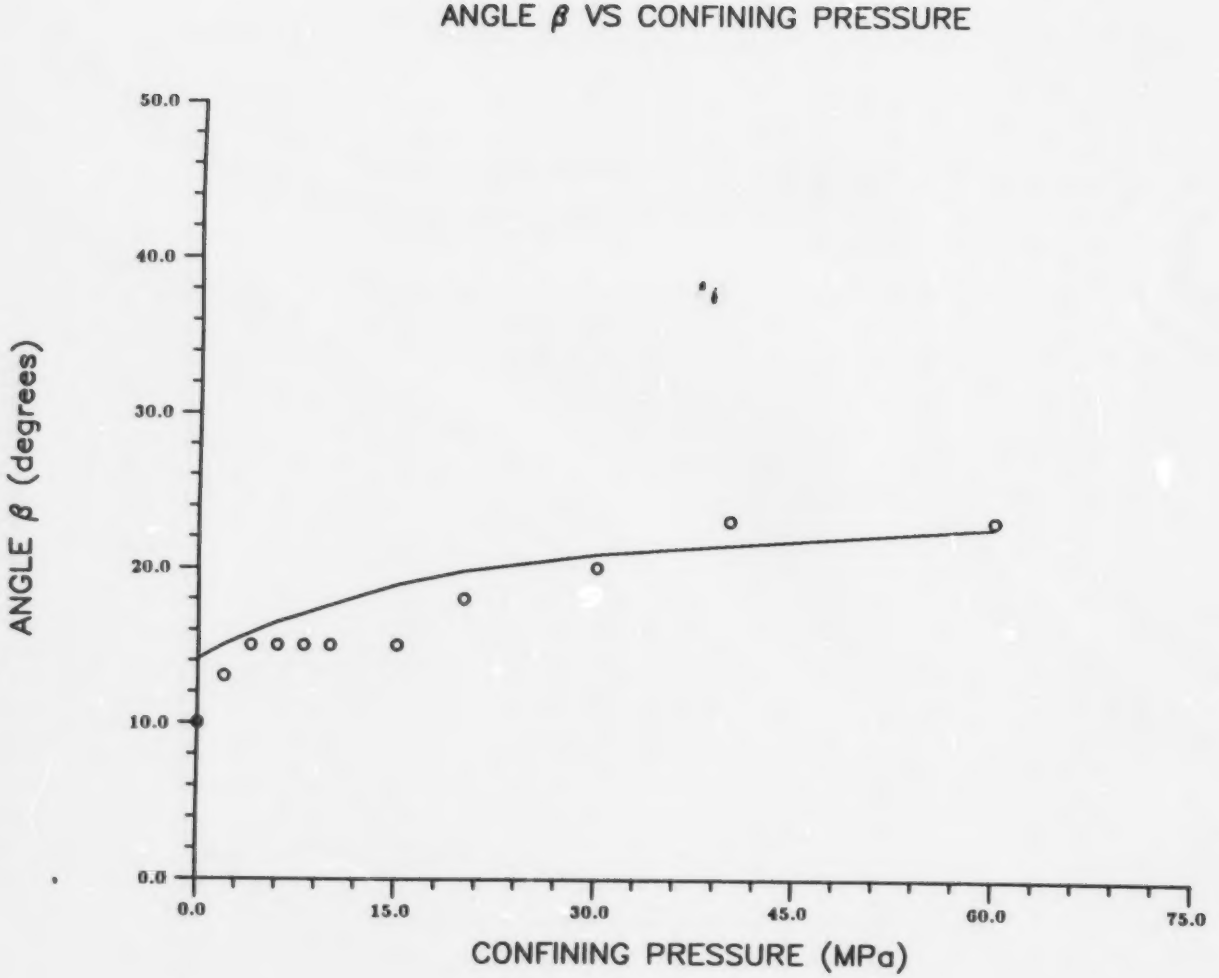

Figure 15. Plots of angle β versus confining pressure.

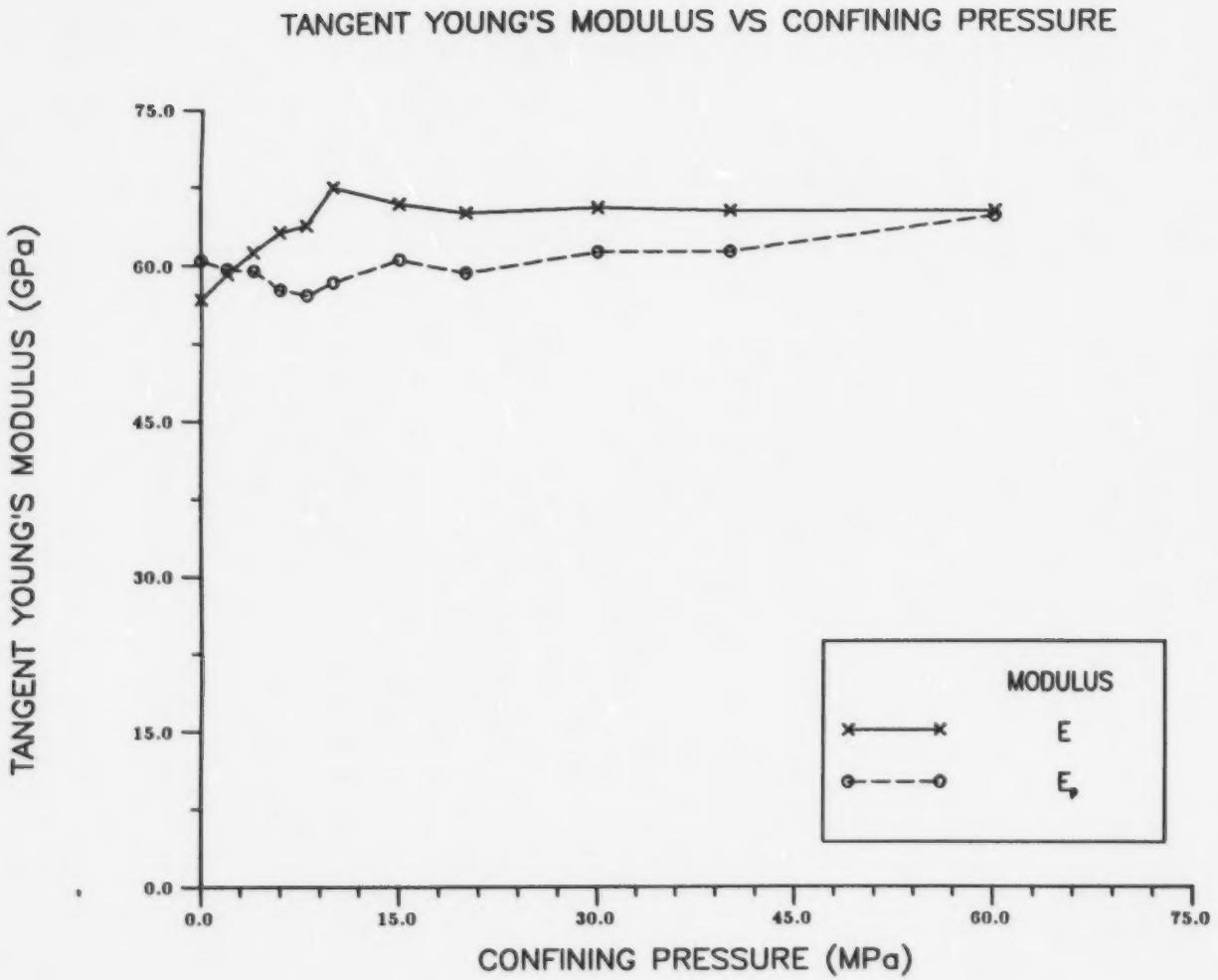

Figure 16. Plots of tangent Young's moduli, E and E_p, versus confining pressure.

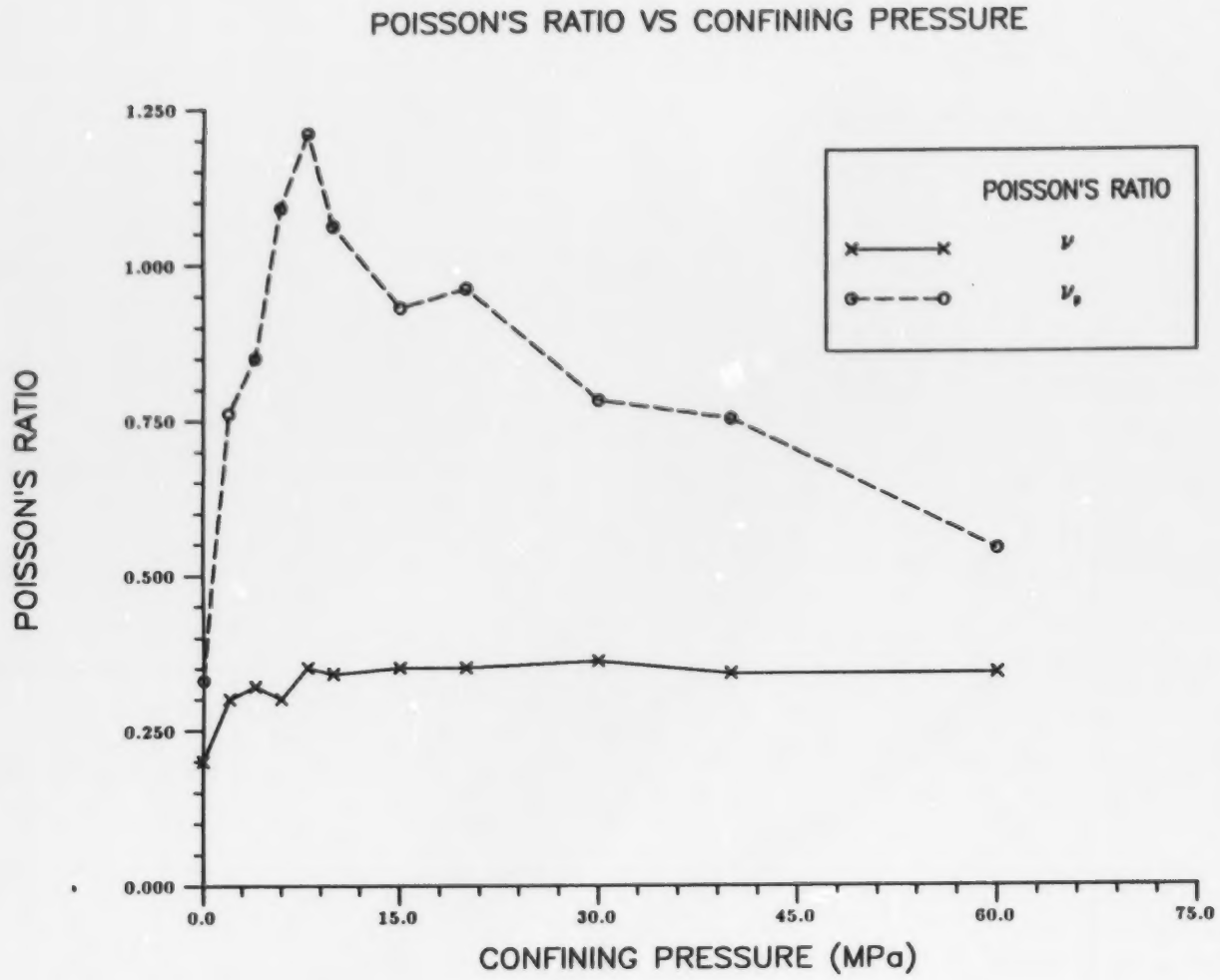

Figure 17. Plots of Poisson's ratios, ν and ν_p, versus confining pressure.

APPENDIX A

Loading-unloading Curves

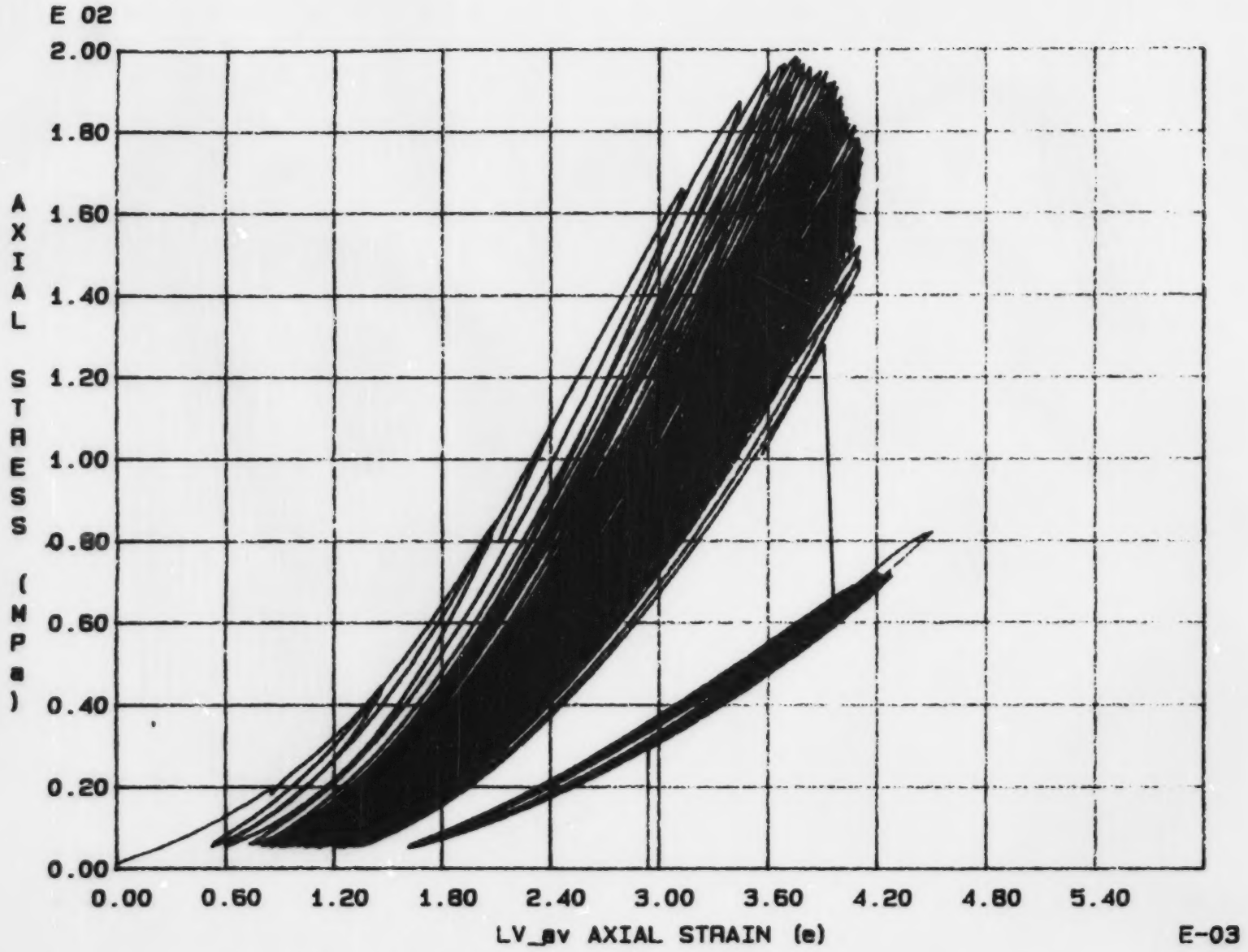

Figure A1. Loading and unloading curves (axial strain) for Specimen MB1-36.070.

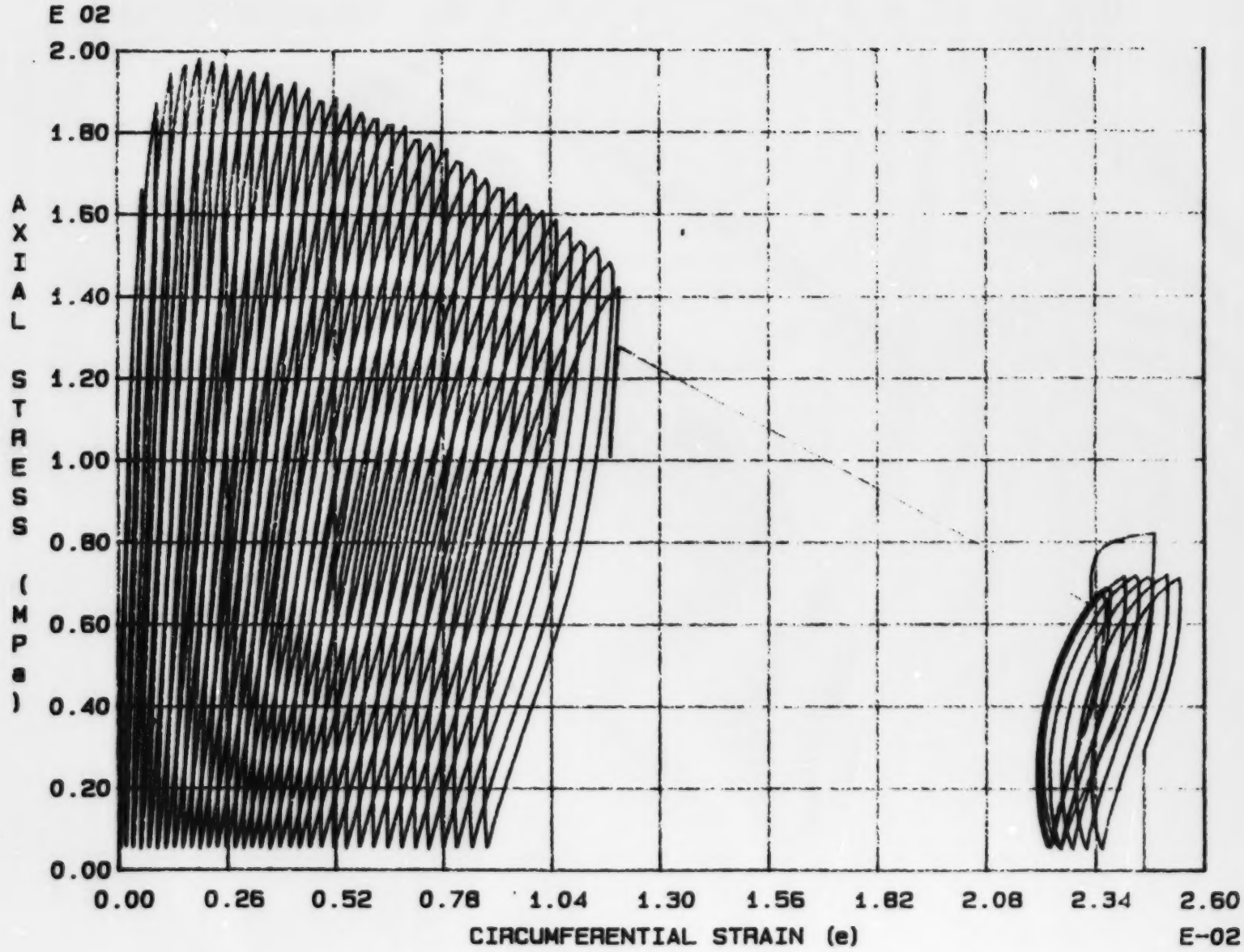

Figure A2. Loading and unloading curves (cir. strain) for Specimen MB1-36.070.

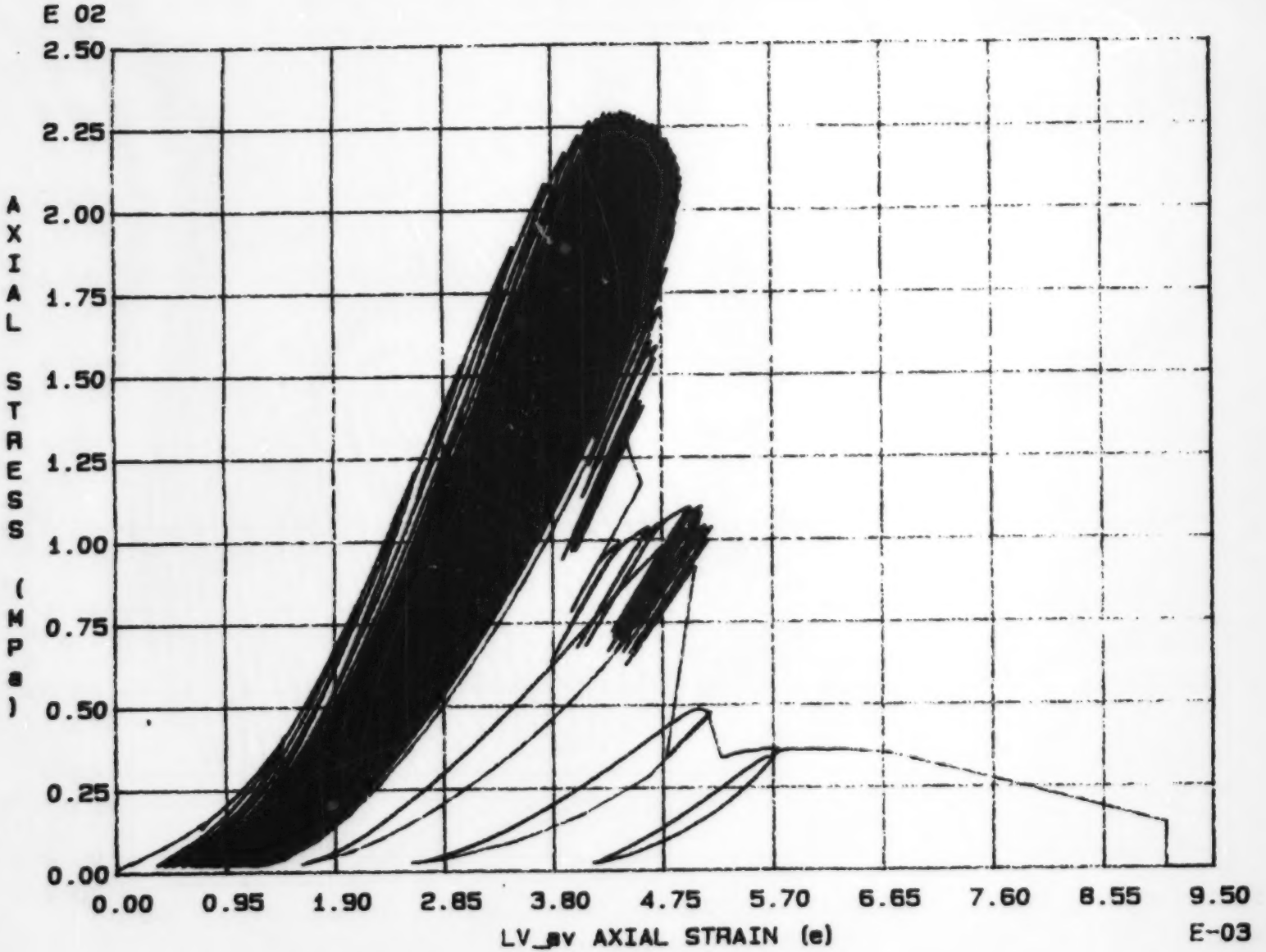

Figure A3. Loading and unloading curves (axial strain) for Specimen MB1-38.207.

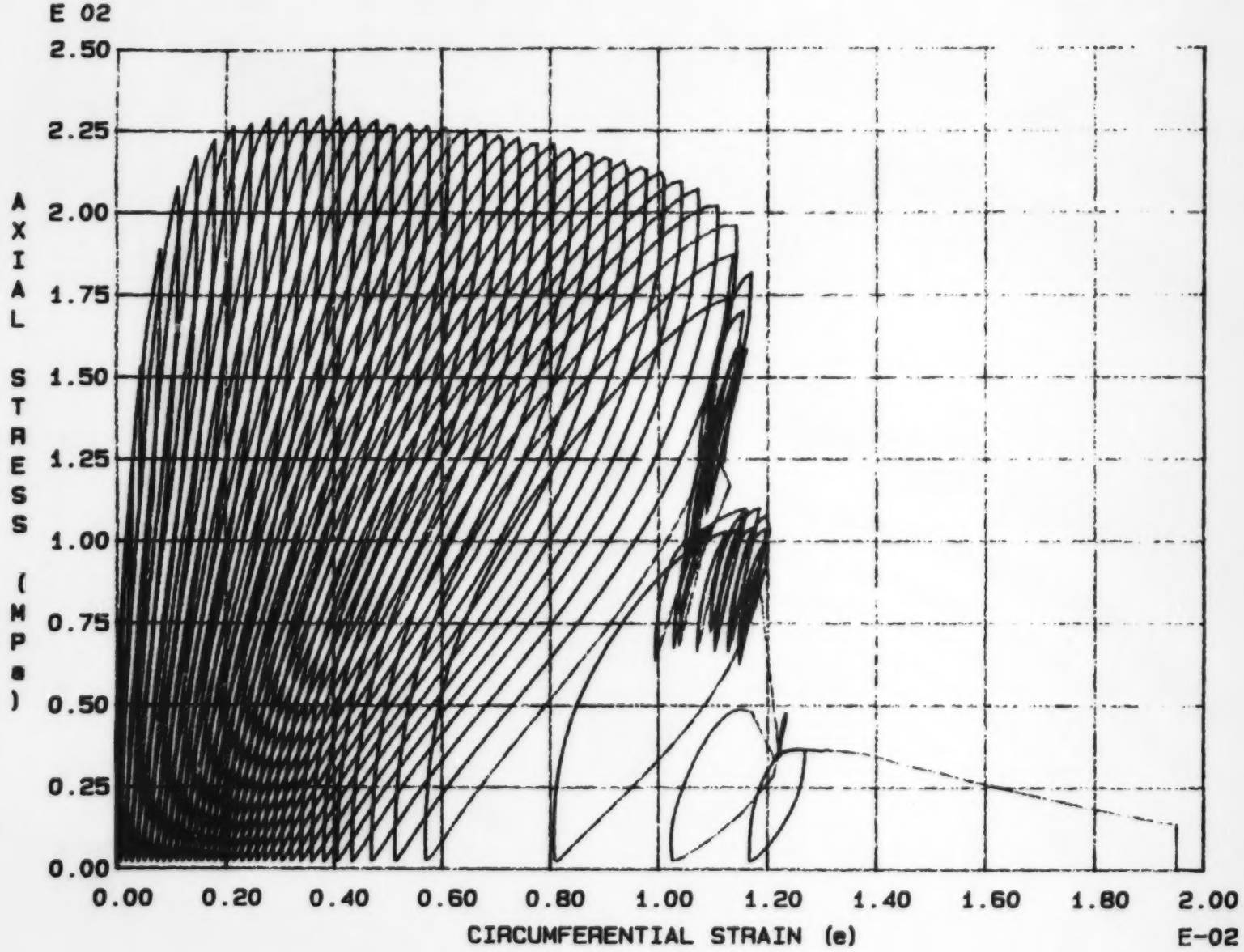

Figure A4. Loading and unloading curves (cir. strain) for Specimen MB1-38.207.

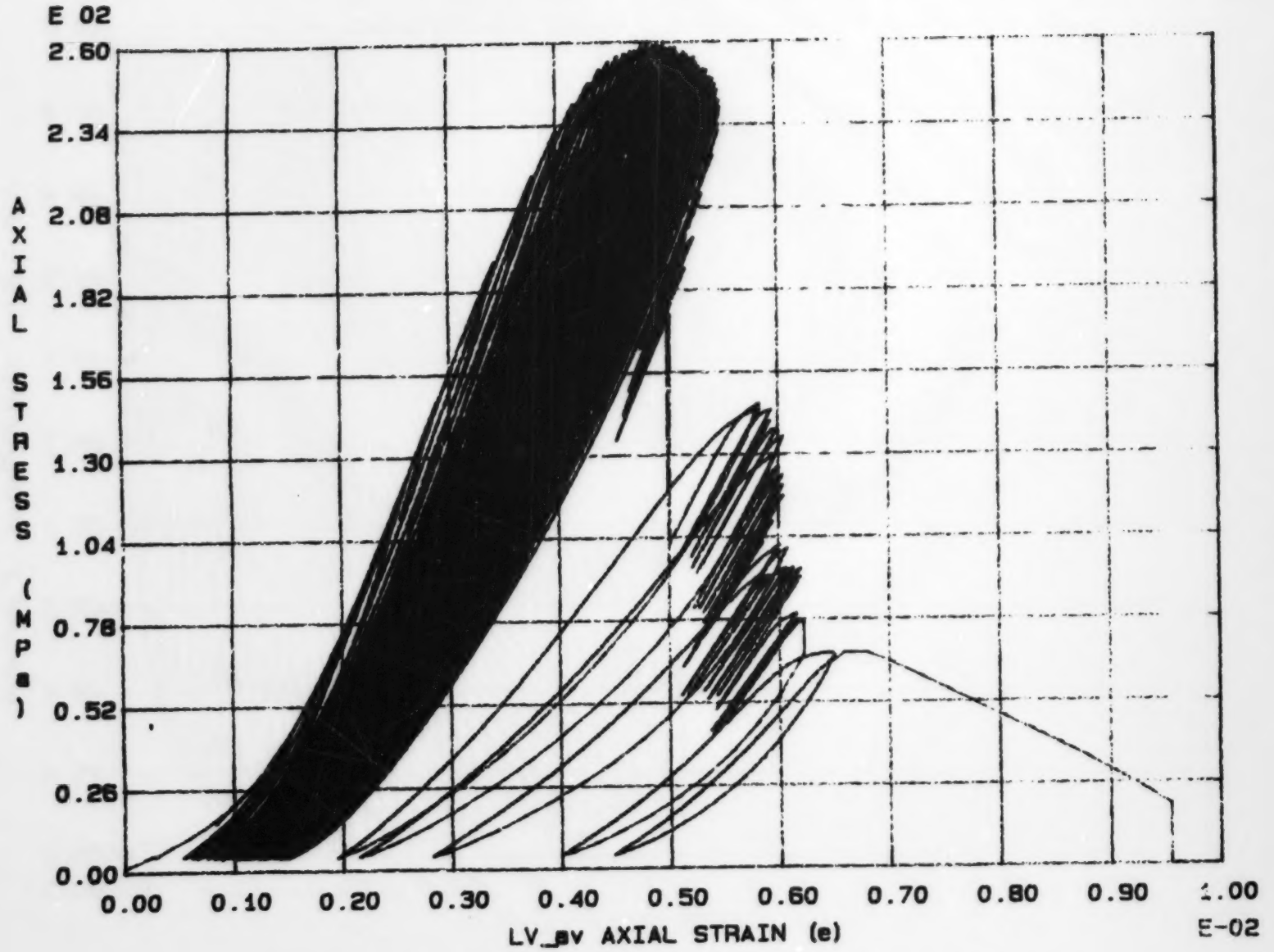

Figure A5. Loading and unloading curves (axial strain) for Specimen MB1-36.373.

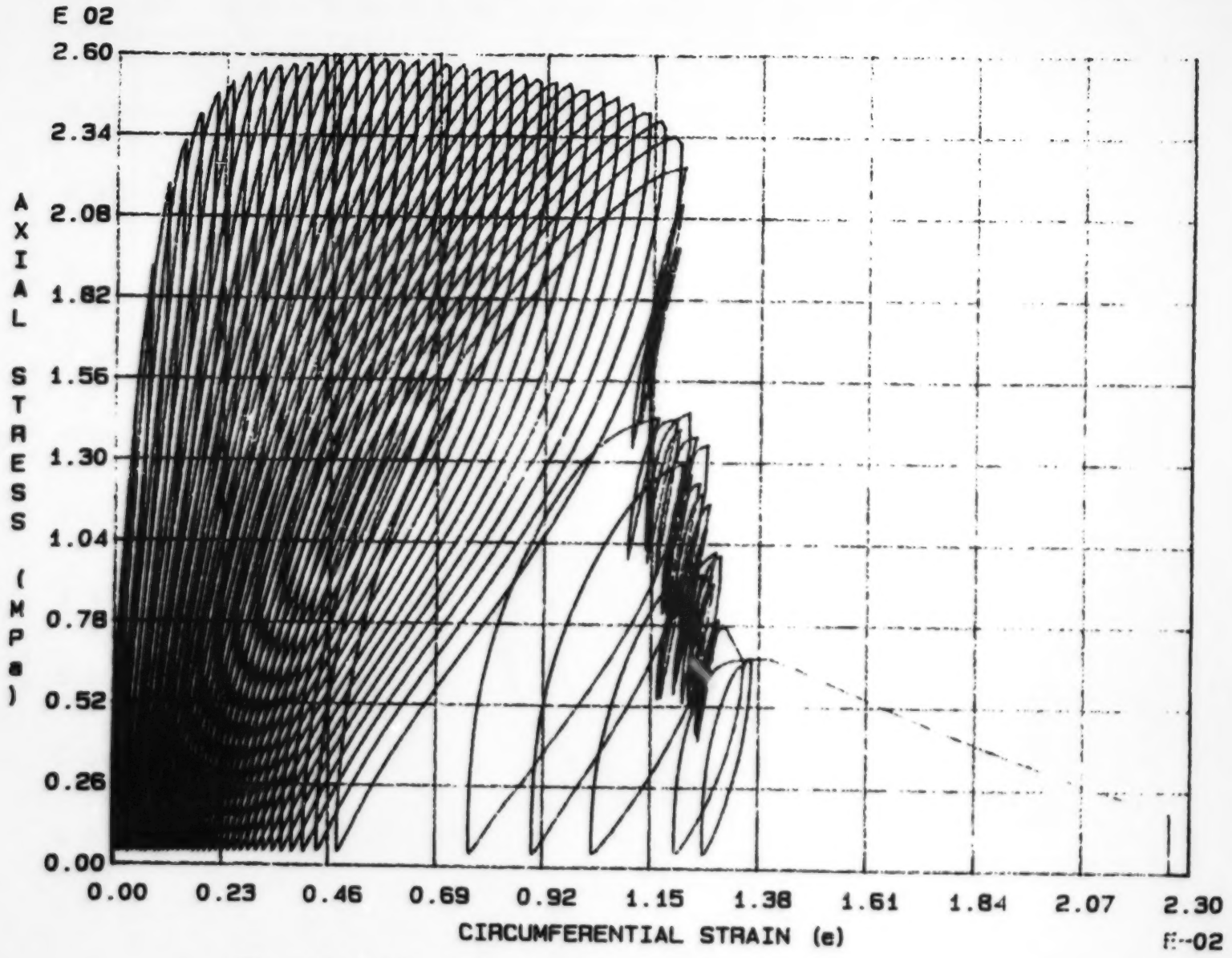

Figure A6. Loading and unloading curves (cir. strain) for Specimen MB1-36.373.

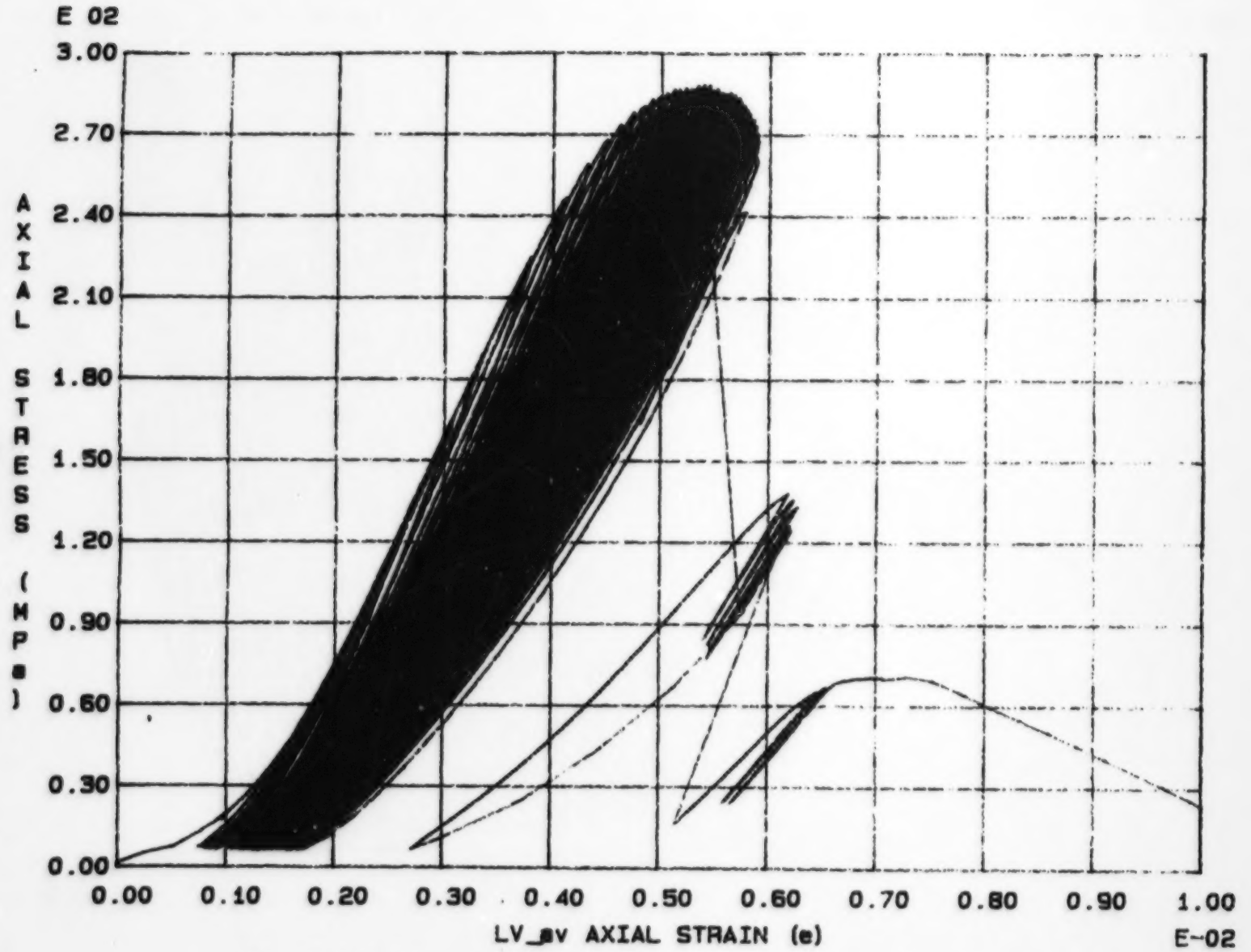

Figure A7. Loading and unloading curves (axial strain) for Specimen MB1-36.529.

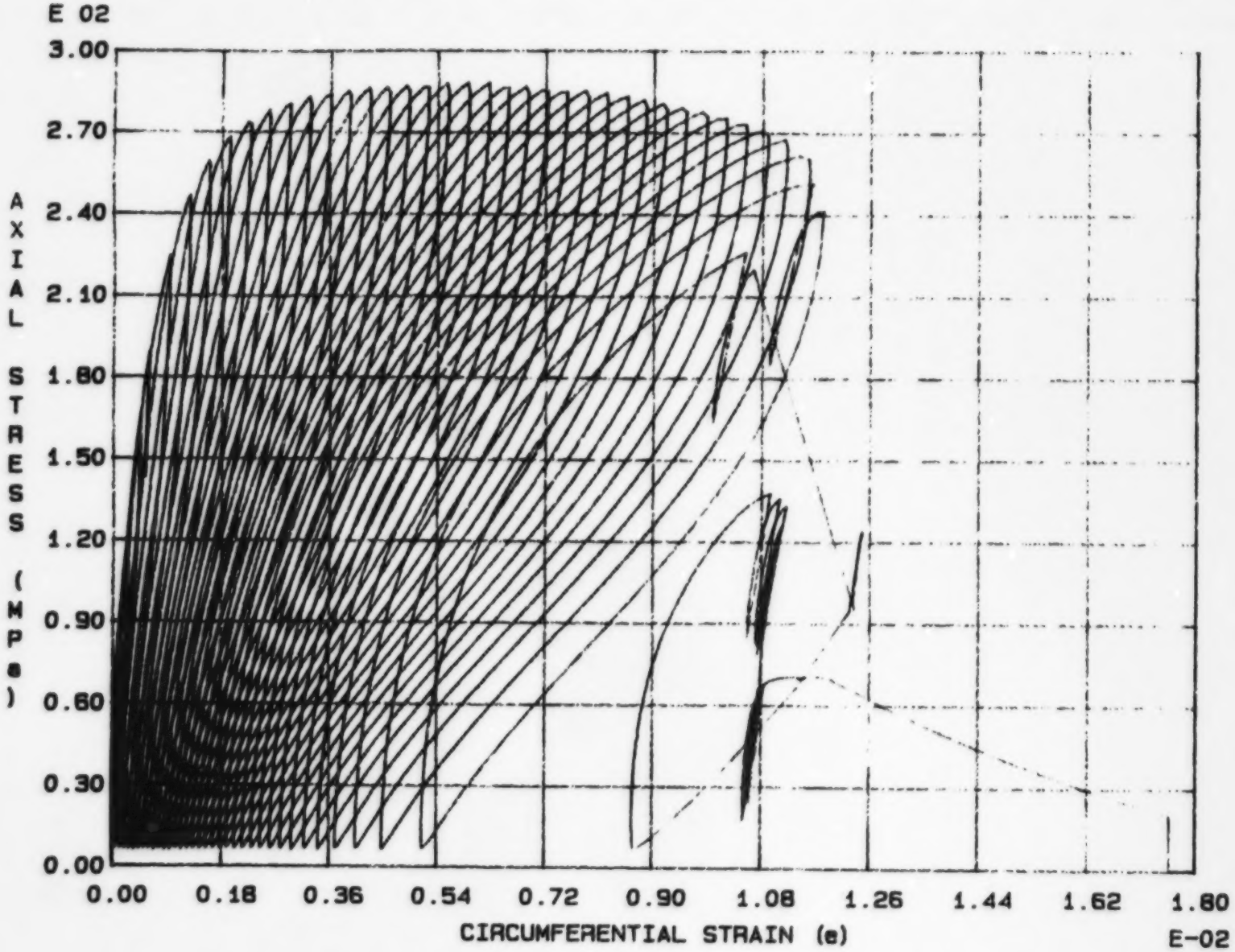

Figure A8. Loading and unloading curves (cir. strain) for Specimen MB1-36.529.

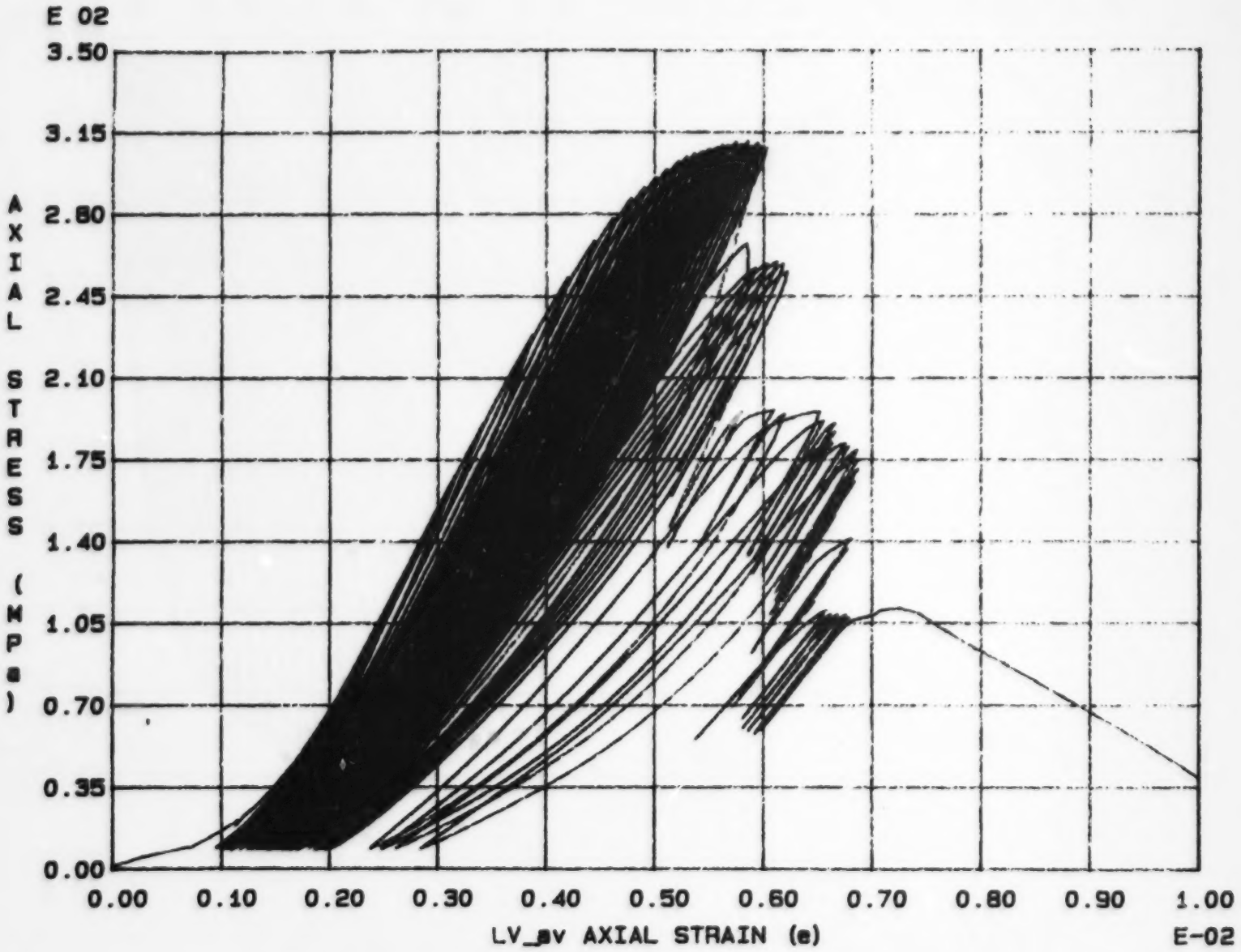

Figure A9. Loading and unloading curves (axial strain) for Specimen MB1-36.687.

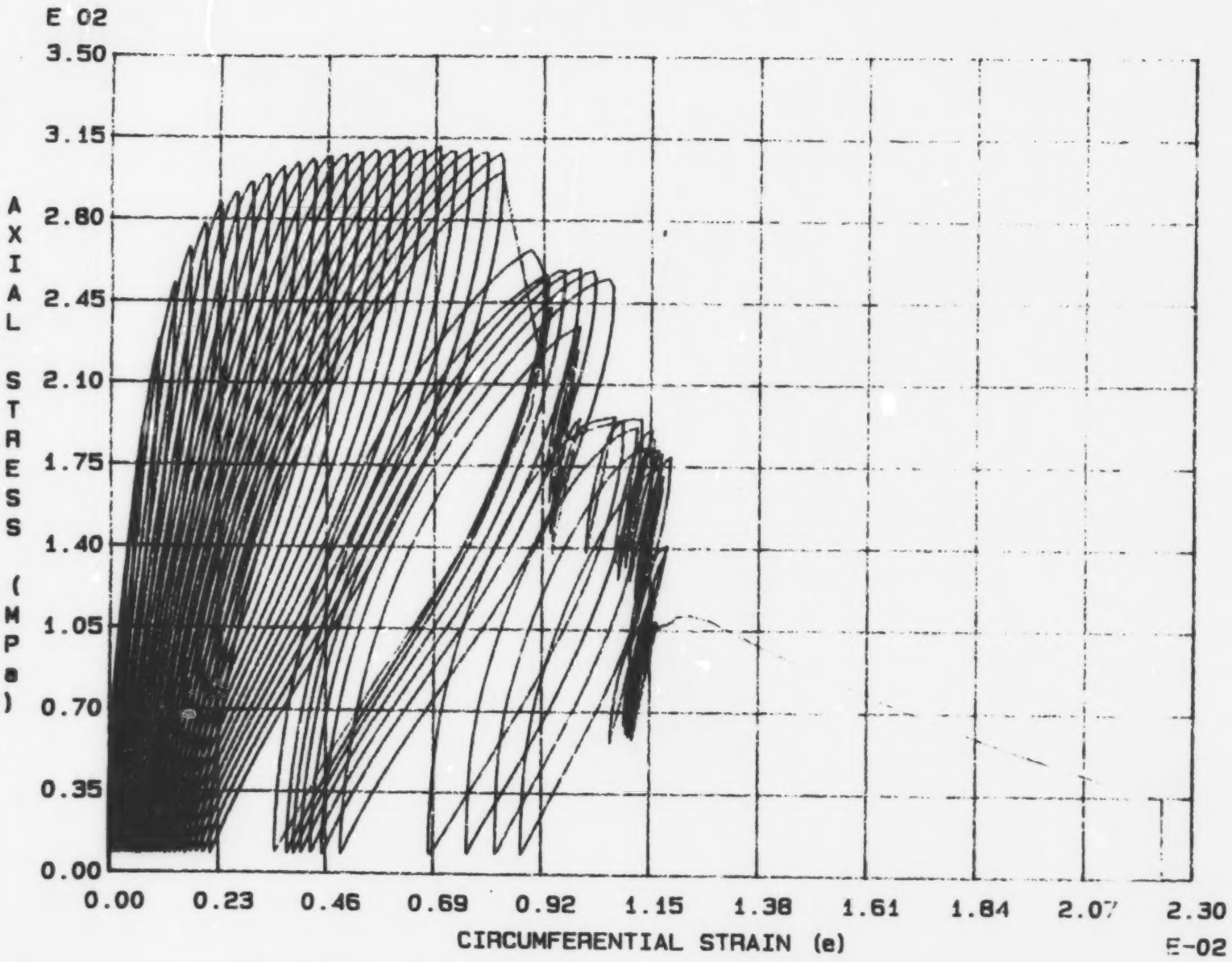

Figure A10. Loading and unloading curves (cir. strain) for Specimen MB1-36.687.

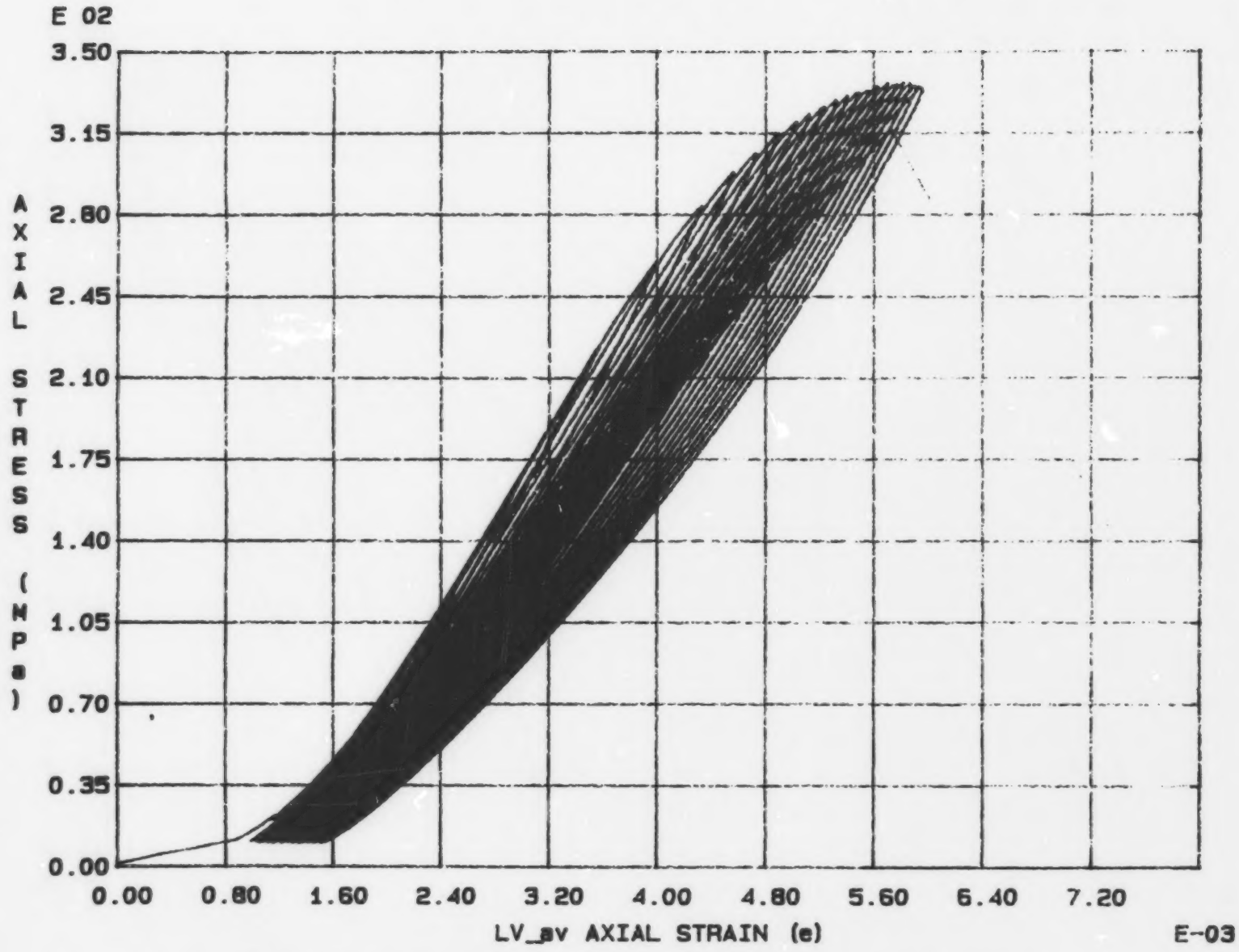

Figure A11. Loading and unloading curves (axial strain) for Specimen MB1-37.000.

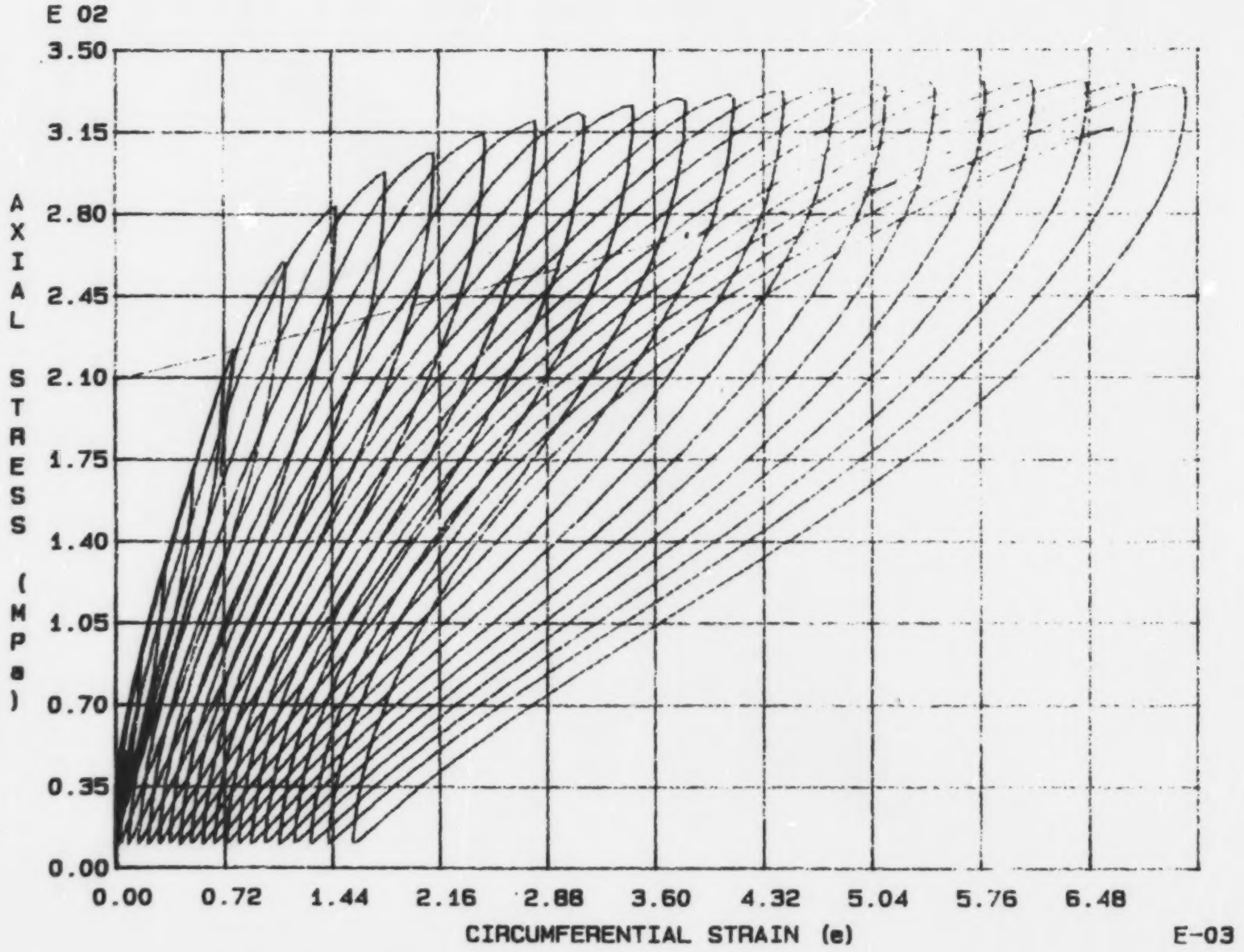

Figure A12. Loading and unloading curves (cir. strain) for Specimen MB1-37.000.

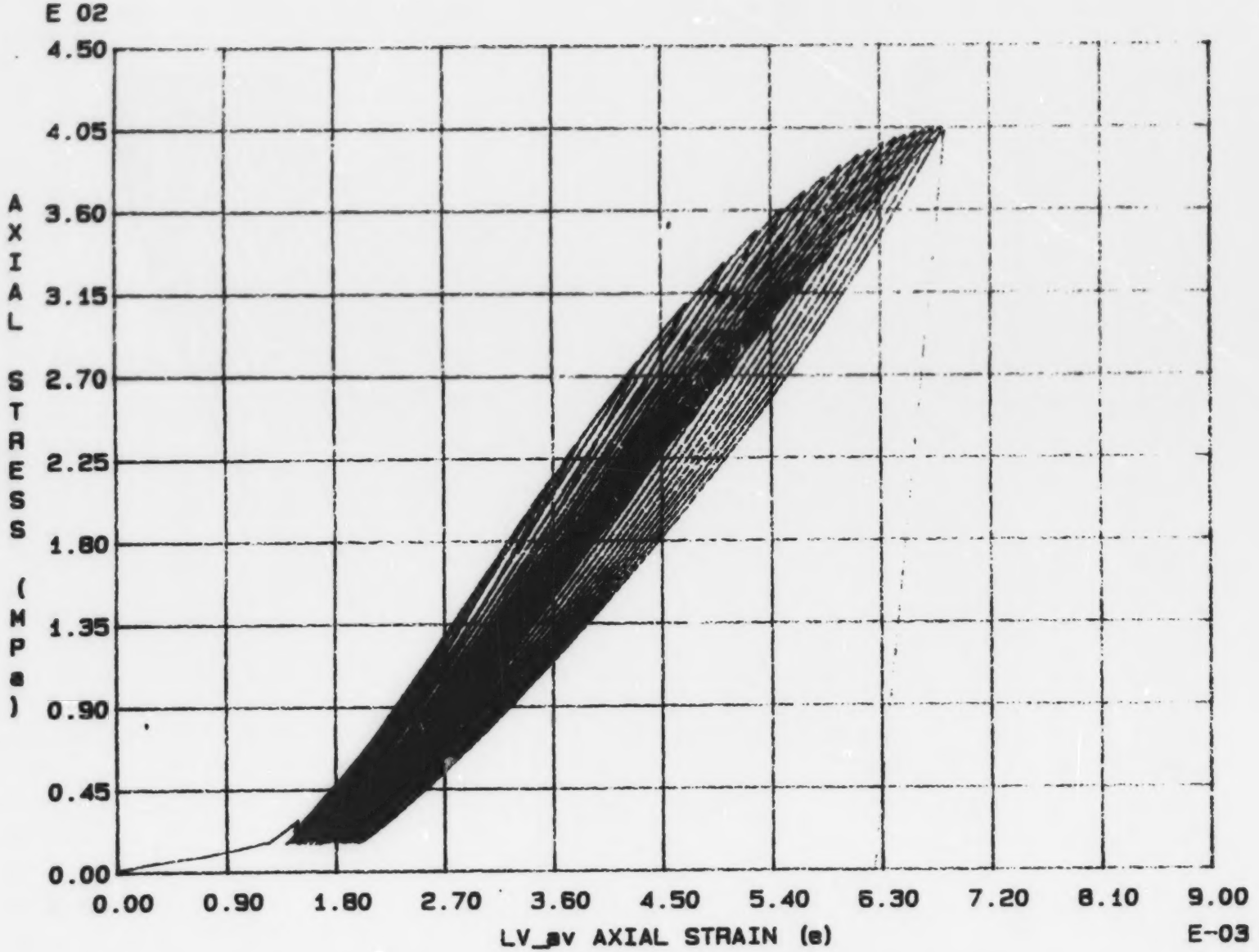

Figure A13. Loading and unloading curves (axial strain) for Specimen MB1-37.156.

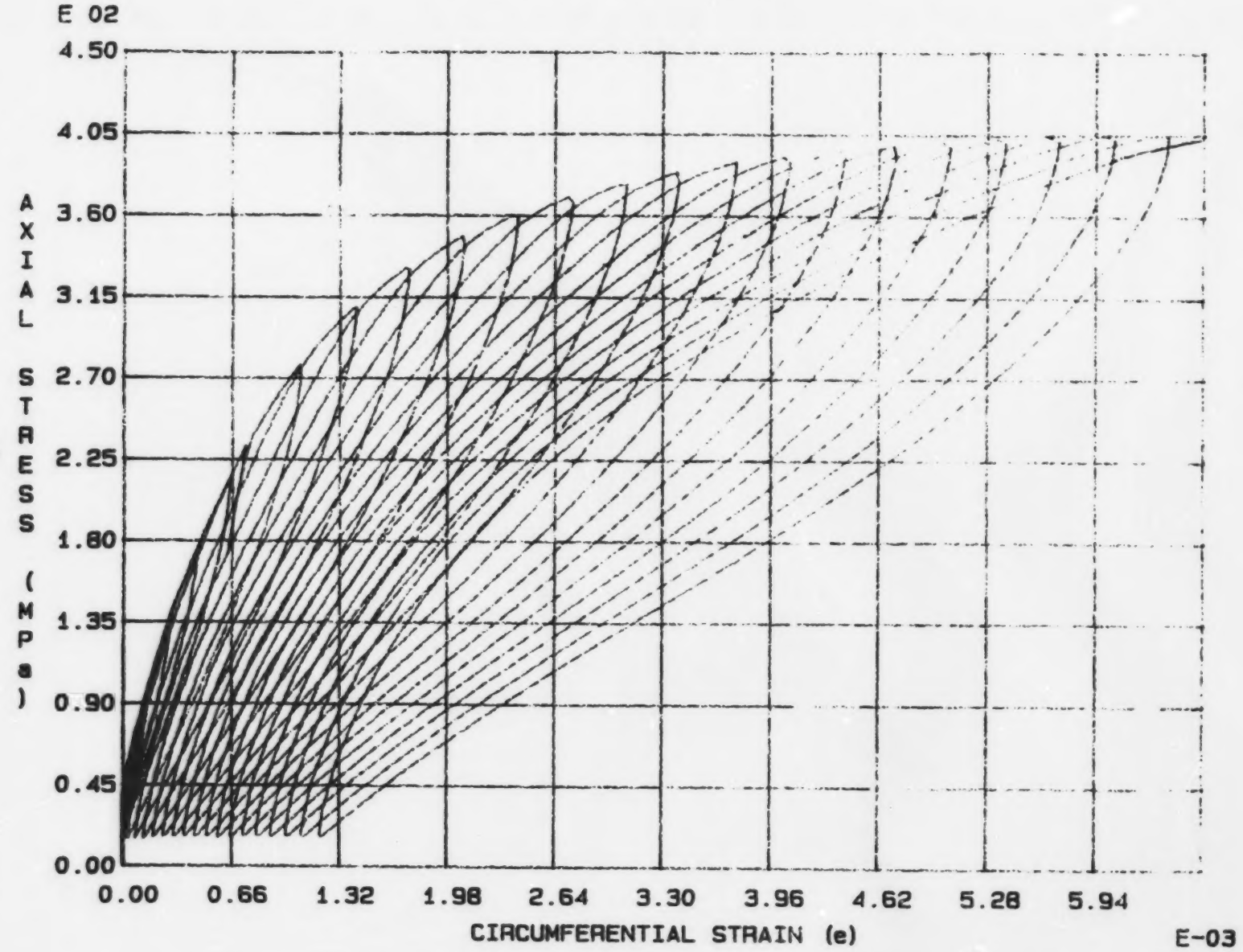

Figure A14. Loading and unloading curves (cir. strain) for Specimen MB1-37.156.

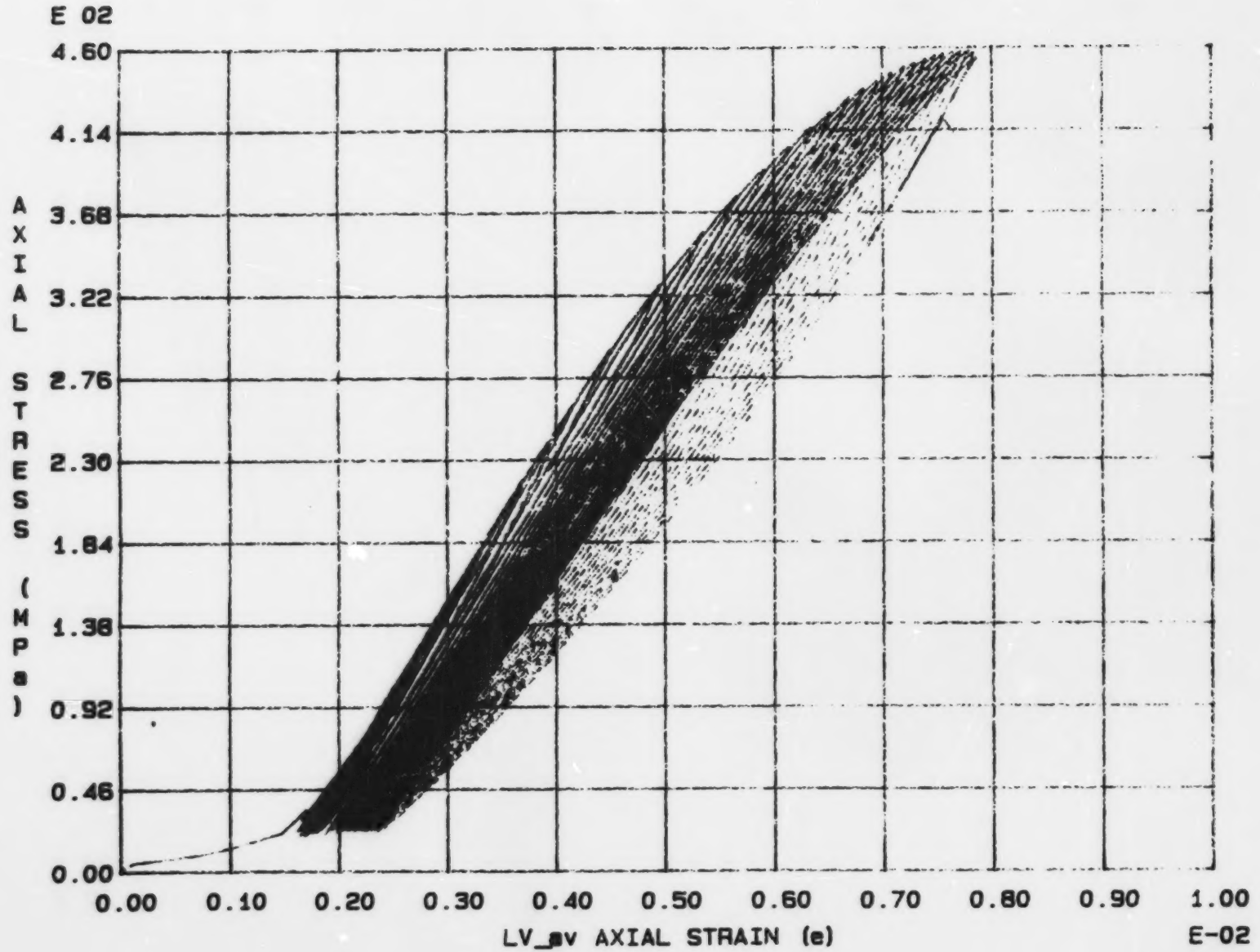

Figure A15. Loading and unloading curves (axial strain) for Specimen MB1-37.343.

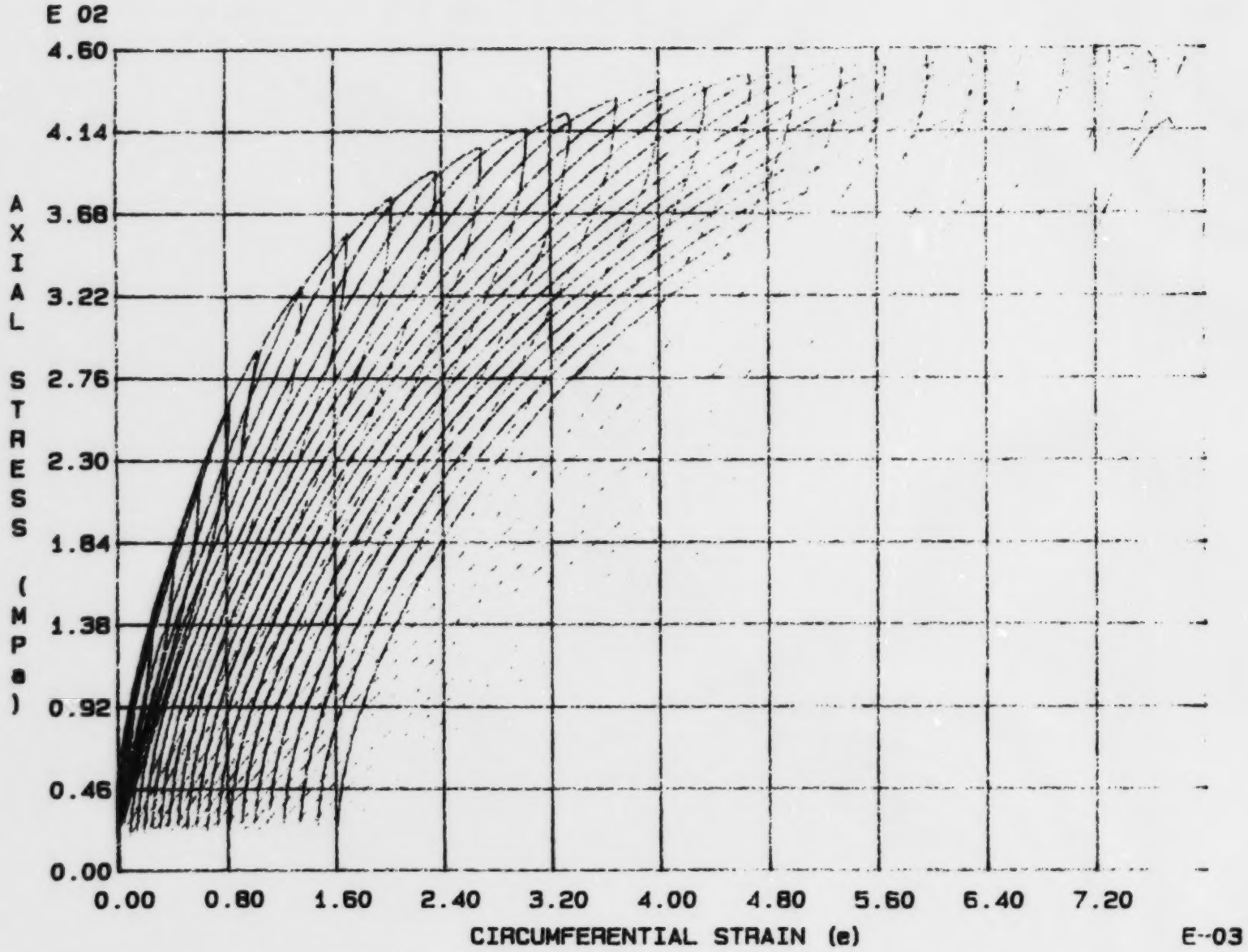

Figure A16. Loading and unloading curves (cir. strain) for Specimen MB1-37.343.

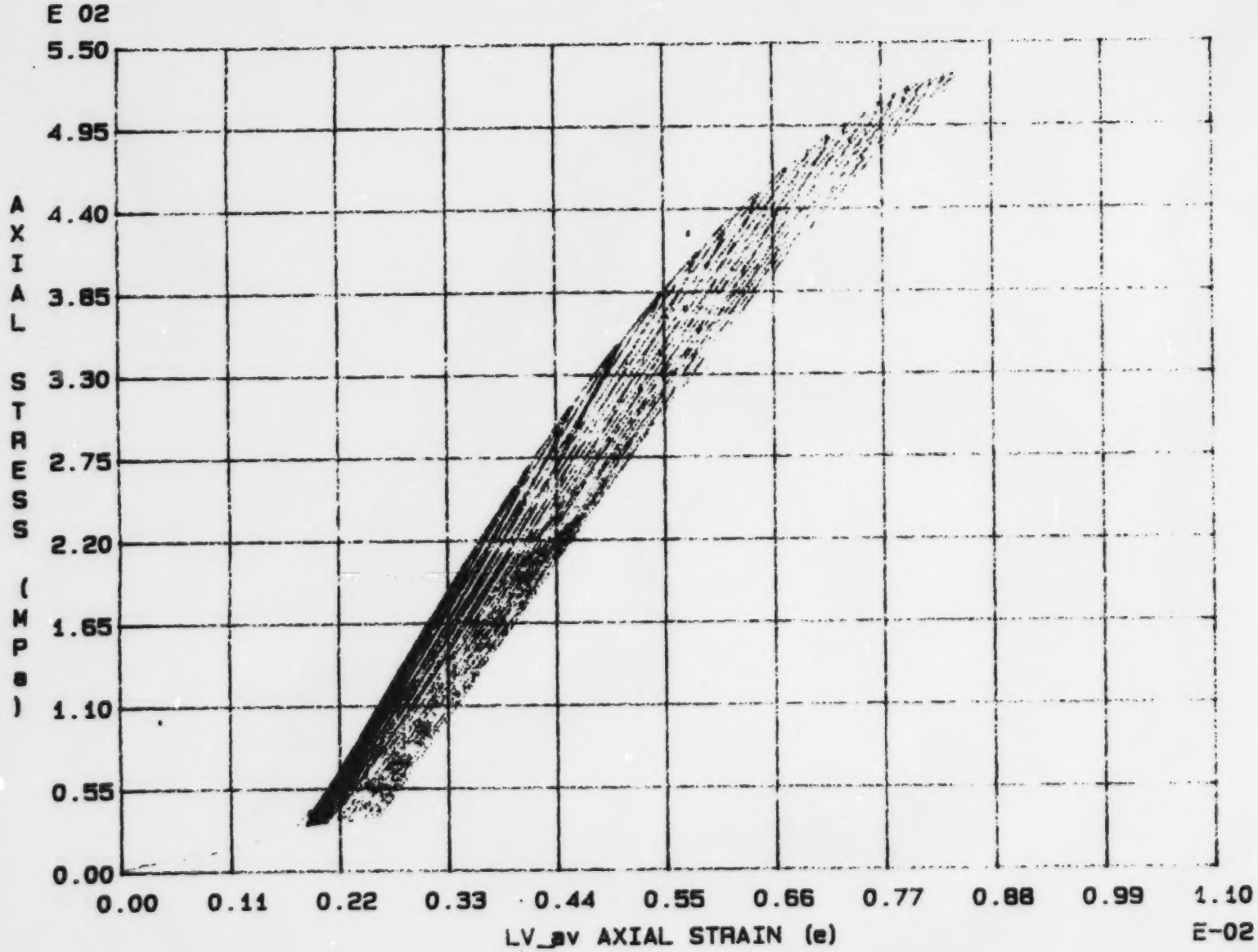

Figure A17. Loading and unloading curves (axial strain) for Specimen MB1-37.502.

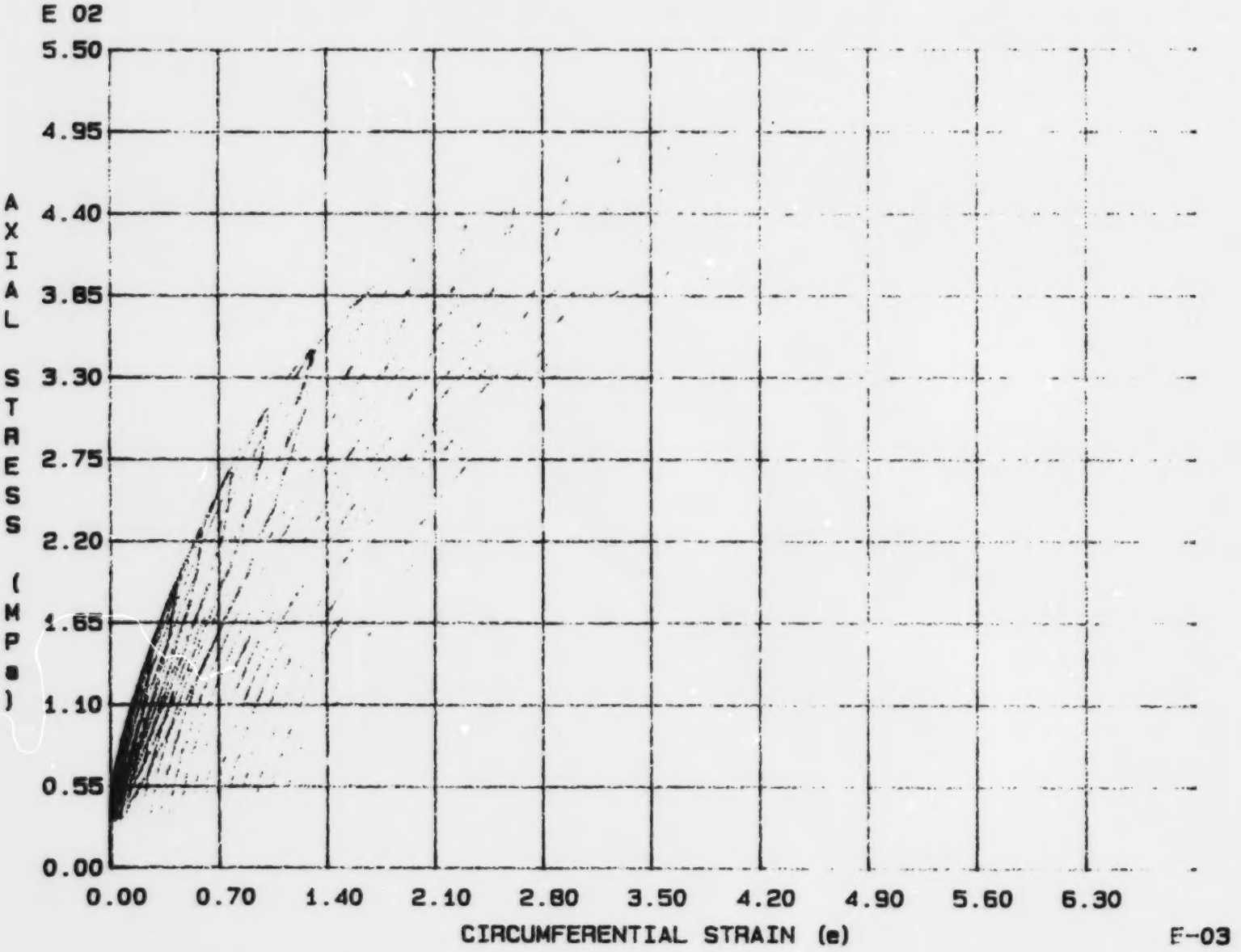

Figure A18. Loading and unloading curves (cir. strain) for Specimen MB1-37.502.

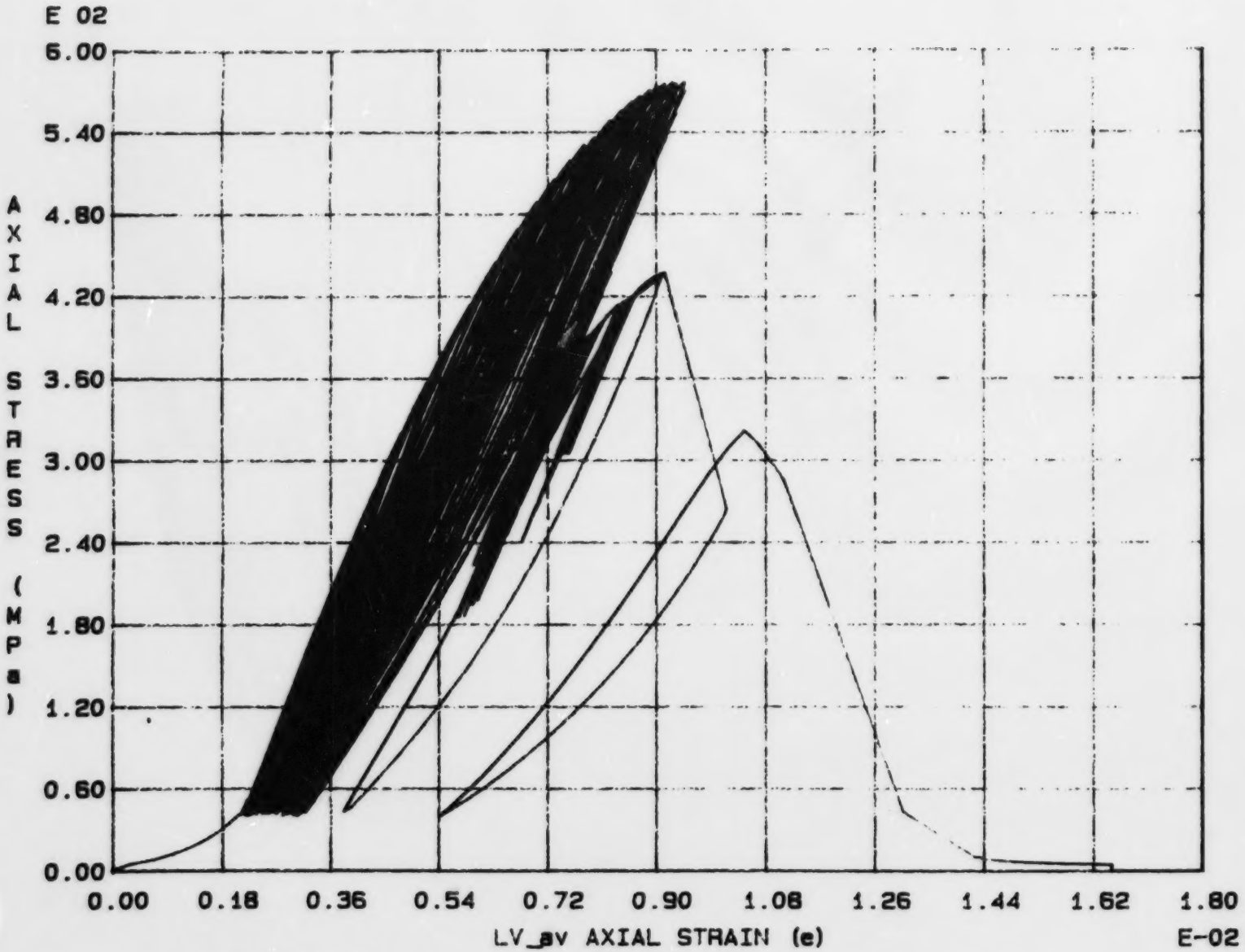

Figure A19. Loading and unloading curves (axial strain) for Specimen MB1-37.650.

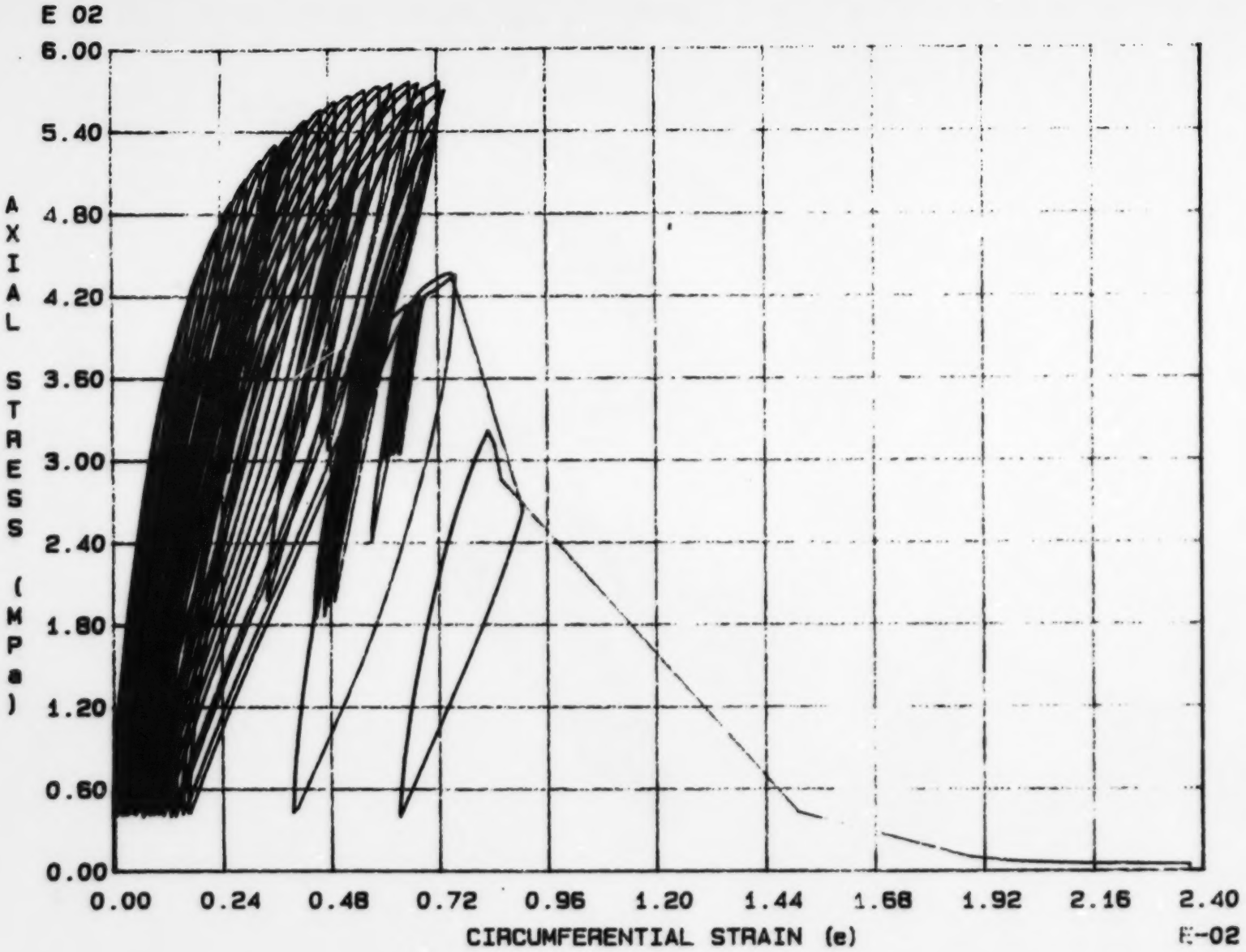

Figure A20. Loading and unloading curves (cir. strain) for Specimen MB1-37.650.

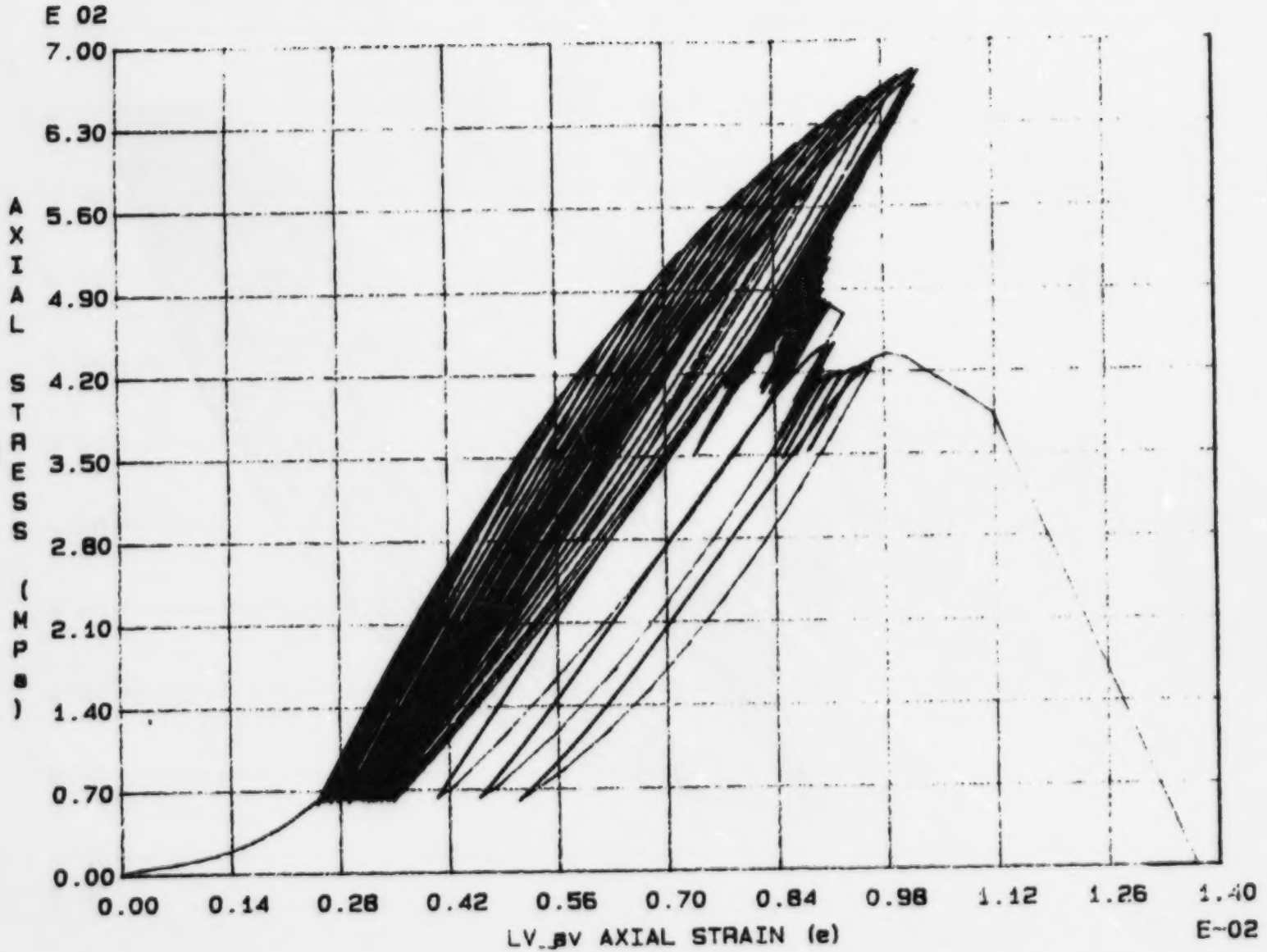

Figure A21. Loading and unloading curves (axial strain) for Specimen MB1-37.805.

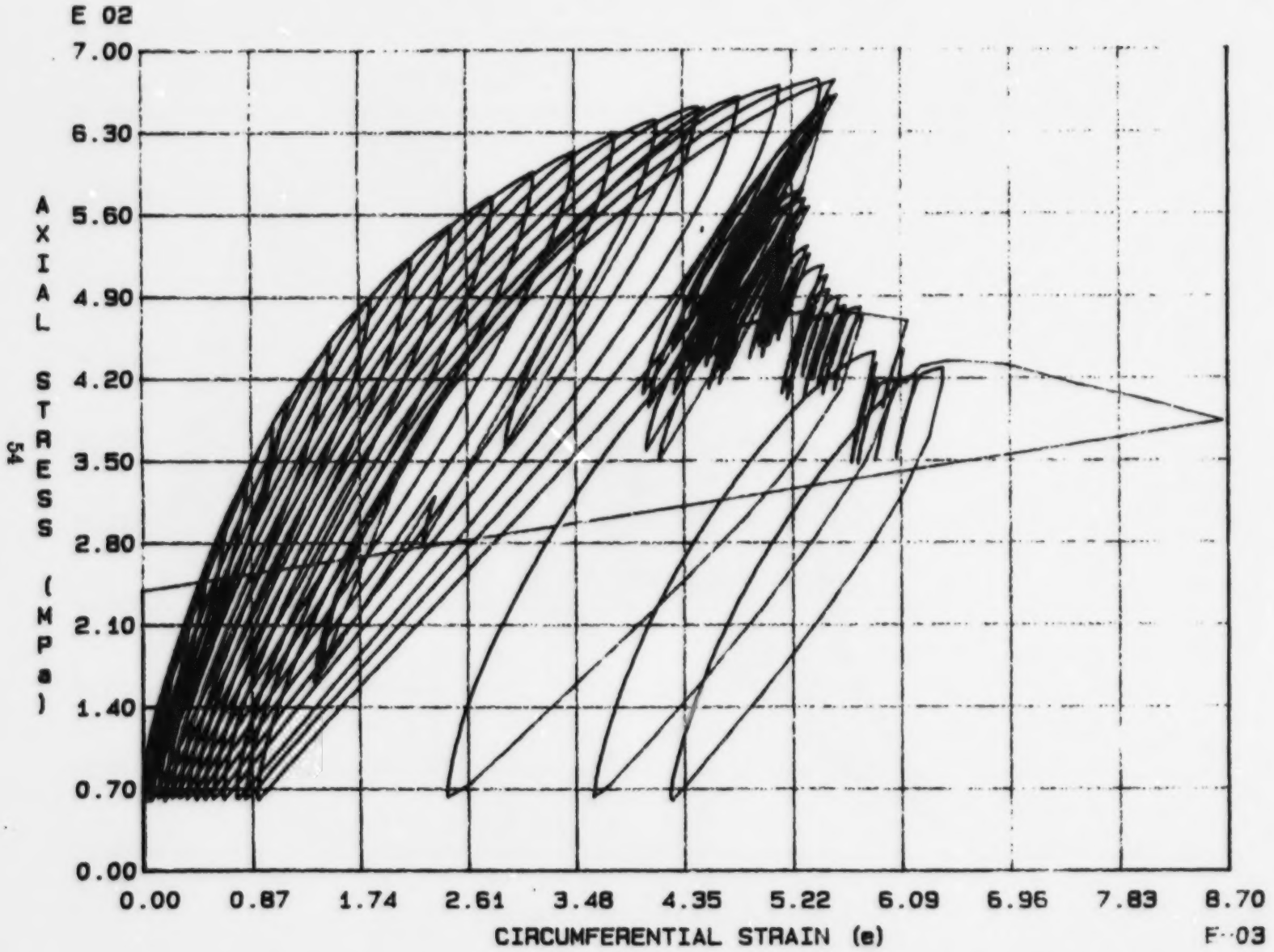

Figure A22. Loading and unloading curves (cir. strain) for Specimen MB1-37.805.